UNIVERSITY OF CENTRAL OKLAHOMA

Edmond, Oklahoma

Jackson College of Graduate Studies

FROM CANCER TO FORESNICS: THE IMMUNOHISTOCHEMICAL CHARACTERIZATION OF TP63, TP53, and MDM2 PROTEINS TISSUE EXPRESSION IN SKIN BASAL CELL AND SQUAMOUS CELL CARCINOMAS.

A THESIS

SUBMITTED TO THE GRADUATE FACULTY

In partial fulfillment of the requirements

For the degree of

MASTER OF SCIENCE IN FORENSIC SCIENCE

By

Mohamed Amine Khadiri

Edmond, Oklahoma

2020

Thesis Title

Mohamed Amine Khadiri

Author's Name

12/02/2020

Date

Jackson College of Graduate Studies at the University of Central Oklahoma

A THESIS APPROVED FOR

THE W. ROGER WEBB FORENSIC SCIENCE INSTITUTE

By

Wayne D. Lord Digitally signed by Wayne D. Lord Date: 2020.12.02 12:31:19 -06'00'

Committee Chairperson

Ruth H. Oneson Digitally signed by Ruth H. Oneson Date: 2020.12.03 10:37:05 -06'00'

Committee Member

James Creecy Digitally signed by James Creecy Date: 2020.12.03 14:50:45 -06'00'

Committee Member

Melville B. Vaughan, Ph. D. Digitally signed by Melville B. Vaughan, Ph. D. Date: 2020.12.04 12:03:06 -06'00'

Committee Member

THESIS ABSTRACT

University of Central Oklahoma

Edmond, Oklahoma

NAME: Mohamed Amine Khadiri

TITLE OF THESIS: From Cancer to Forensics: The Immunohistochemical Characterization of TP63, TP53, and MDM2 Proteins Tissue Expression in Skin Basal Cell and Squamous Cell Carcinomas.

DIRECTOR OF THESIS: Dr. Wayne D. Lord Ph.D.

COMMITTEE MEMBERS: Dr. Ruth H. Oneson MD, MPH.
Dr. James Creecy Ph.D.
Dr. Melville B. Vaughan Ph.D.

PAGES: 101

ABSTRACT: Skin cancer is one of the most occurring cancers in the world and its occurrence is rising. Many factors contribute to the development of skin cancers such as UV light exposure, chronic inflammation, and genetic susceptibility. Cancers such as basal cell carcinomas and squamous cell carcinomas arise from cells within the epidermis. TP53 and TP63, members of the p53 protein family, play a major role in skin tumorigenesis and progression. While p53 is the most mutated gene in human cancers, p63 is seldom mutated in cancers. The functions of p53, “guardian of the genome”, have been well documented and studied. Nonetheless, many studies show that p63 is overexpressed in tumors. Other studies show that p63 is lost during tumorigenesis and cancer progression. Consequently, whether the p63 gene is a tumor suppressing gene or an oncogene remains a matter of the p63 protein’s isoforms present in these tumors and their interactions with p53 and MDM2. This challenge has two facets. First, the multiple spliced isoforms of p53 and p63 which have different functions in skin development as well as skin cancers.

Second, the Mouse Double Minute 2 (MDM2) protein, a negative regulator of p53, which has been shown to have different proteomic affinities by which it binds these different p53 and p63 isoforms. The findings of this project are geared toward characterizing and semi-quantifying the histopathological expression of p63, p53 and MDM2 in cutaneous basal cell carcinomas as well as squamous cell carcinomas, while addressing the aggregation propensities between these proteins. The project also aims to summarize the forensic use of p53 and p63 as potential biomarkers for the estimation of age in antemortem and postmortem wounds and lesions. We have used advanced softwares such as ImageJ from the NIH and QuPath to extract important data to better characterize the layer-by-layer expression of p53, p63, and MDM2 in specific areas such as the epidermis, the dermal layer, stroma, and tumor nests. We used multiple skin tumor biopsies and excisions from three different skin cancer patients. The molecular simulations using the PASTA 2.0, AGGRESCAN, and FELLS webservers is to compare and contrast the aggregation propensities of p53 and p63 and what locations of their protein sequences are hot spots for aggregation. Results showed that p63 has the most stain intensity and was strictly nuclear in all three cases (p-value of 0.0007). The consistent expression of p63 in all three cases indicates the important role of p63 in the tumorigenesis of skin epithelial cells and dysplasia. MDM2 has been shown to have a strong stain intensity both nuclear and cytoplasmic in all three cases but was of no significance in differentiating our cases (p-value of 0.718). p53 was partially absent in all three cases and had a weak stain intensity when present (p-value of

0.086). Data from the FELLS, PASTA 2.0, and AGGRESCAN showed that p53 has the highest number of residues susceptible to aggregation at 27.48% (108 residues), whereas p63 and MDM2 have aggregation percentages of 7.94% (54 residues) and 3.67% (18 residues) respectively. Clinically, studies show that p63, particularly the ΔNp63 isoform, has an essential role in epithelial wound repair. Forensically, studies show that p53's expression increased in wounds with an interval of post-infliction of three to 77 days. This makes p53 a potential candidate for wound age estimation in ante-mortem wounds with longer survival time after the injury. Research also shows that these later conclusions cannot be applied to postmortem wounds and that further research is needed to evaluate the potential use of p53 in a postmortem setting.

I declare that the work I am submitting herein contains no section copied in whole or in part from any other source unless explicitly identified in quotation marks and with detailed, complete, and accurate references.

Acknowledgement

First and foremost, I would like to truly thank members of my graduate research committee for the opportunity to do research, their trust, and their mentorship. I would not have been able to accomplish any of this without them. I would like to thank Dr. Wayne Lord for his continuous support and guidance through the length of my graduate studies. I would like to thank Dr. Ruth Oneson for the opportunity to work in her pathology laboratory and for the opportunity to conduct this project as a coordination between Heartland Pathology Consultants Edmond USA, the University of Central Oklahoma, and the W. Roger Webb Forensic Science Institute. I would like to thank Dr. James Creecy and Dr. Melville Vaughan for their support and focused feedback about this project. I have had the honor to have attended the University of Central Oklahoma both as an undergraduate and graduate student. Hence, I would like to thank members of the faculty at the UCO's Biology Department and at the W. Roger Webb Forensic Science Institute for their teaching and their passion about science and research. I have made lifelong relationships and friendships and have learned many valuable lessons which I will cherish for life. Thank you all for what you do for science, students, and academia.

To my family, I would like to say thank you for your unconditional love and support. I hope that the 18-year-old who took a chance at coming to this great country is now a man who make you proud.

RESPECTFULLY AND THANK YOU ALL!

TABLE OF CONTENTS

Ethics and Considerations

The Formalin-Fixed Paraffin-Embedded samples were taken as the main materials for this study, which uses surgically removed skin biopsies of Basal cell Carcinomas (BCCs) and Squamous Cell Carcinomas (SCCs) from patients with approval of both the Institutional Review Board (IRB) and the laboratory medical director's consent. The archival pathology Formalin Fixed Paraffin Embedded (FFPEs) blocks were obtained from Heartland Pathology Consultants Edmond, Oklahoma under the supervision of Dr. Ruth Oneson MD, MPH (pathologist and medical director) regarding all the Health Insurance Portability and Accountability Act (HIPPA) regulations to protect patient information and privacy. All documents supporting the ethics of this study were submitted to the research committee.

List of Figures

List of Tables

List of Abbreviations

AGGRESCAN: Aggregation Scan (web server)

BCC: Basal Cell Carcinoma

DAB: 3,3′-Diaminobenzidine stain

DBD: DNA Binding Domain

DN: Domain Negative

FELLS: Fast Estimator of Latent Local Structure

FFPE: Formalin Fixed Paraffin Embedded

FIJI: FIJI Is Just ImageJ (software)

H/E: Hematoxylin and Eosin

IHC: Immunohistochemistry

LoF: Loss of Function

MDM2: Murine (Mouse) Double Minute 2

NIH: National Institute of Health

PASTA 2.0: Predicts Amyloids Structural Aggregation 2.0 (web Server)

PMDs: Protein Misfolding Diseases

PrP: Prion Protein

QuPath: Quantitative Pathology

RGB: Red, Green, and Blue.

ROI: Region Of Interest

SCC: Squamous Cell Carcinoma

TAp63: Transactivated p63 (TA domain, full length Protein)

WSI: Whole Slide Image

∆**Np63**: Truncated p63 (lack the TA domain)

Project Importance and Field Contributions

Over five million people are diagnosed with basal cell and squamous cell carcinomas every year. The findings of this project are to expand our understanding of the specific proteins' tissue expression, aggregation, and the effects of these proteins on cutaneous tumorigenesis, cancer progression, and downstream forensic pathology uses. The importance of this project lies in that it allows for the qualitative and semi-quantitative characterization of tumor tissue expression of p63, p53, and MDM2 in two histologically distinct cancers and to also use skin cancer biopsies as templates for future forensic skin wound age determination studies. These proteins are extensively investigated due to their important functional interactions necessary for tumorigenesis, apoptosis, and potential treatment for many human cancers. The presence of multiple isoforms of both p63 and p53 is another major confounding area in the study of these proteins, which is yet to be investigated by further research. Results can then be compared to and possibly complement previous findings. Both faculty and future UCO students interested in the field of histology, digital image processing, and software-assisted proteomic analyses can use the simplified methodologies herein and adopt them for their research projects.

Rationale and Hypothesis

We hypothesize that since basal cell carcinoma and squamous cell carcinoma are two distinct cancers histologically, then the IHC quantification of p63, p53, and MDM2's protein expression in the skin tissues will be different at the three major skin layers: the epidermis, the dermis, and the subcutaneous layers. The basis behind the hypothesis is that these proteins interact differently with each other depending on the presence or absence of mutant p53, TAp63, and ΔNp63 isoforms. These protein-to-protein interactions and aggregations remain complex to understand and have significant outcomes on tumorigenesis, progression, and prognosis of many cancers.

CHAPTER ONE: THESIS INTRODUCTION

Basal cell carcinoma (BCC) and squamous cell carcinoma (SCC) are the most occurring non-melanoma cancers and their incidence continue to rise (Geller and Annas 2003). The histological features of both BCC and SCC are well documented in the field of pathology and often times proper diagnosis is easily achieved based on clinical information (Ryu et al., 2018). However, Studies such as the one by Ryu et al., (2018) showed that SCCs have a higher chance to be clinically misdiagnosed as BCCs than *Vice versa*. p63 and p73 are homologous proteins of the tumor protein p53 and collectively these transcription proteins make up the p53 protein family (Yang et al., 1999). While both p63 and p73 can bind the p53 DNA promoters and induce processes such as apoptosis and cellular cycle arrest, both proteins have distinct and different functions than those of p53 (Yang et al., 2000). Unlike p53, p63 and p73 have distinct tissue specific patterns of expression mainly in ectodermally-derived tissues such the skin and the nervous system, respectively (Pozniak et al., 2000). During human development, p63 induces the formation of epidermal tissue and the associated structures such as teeth, hair, and glands. In mature skin, p63 maintains the proliferation of epidermal and dermal stem cells which ensures the homeostasis and regeneration. This also ensures the specific commitment of keratinocytes towards terminal differentiation and stratification (Laurikkala et al., 2006) and (Su 2009). On the other hand, p73 is mainly associated with the development and the homeostasis of the nervous system (Pozniak et al., 2002) and (Truong 2006).

Although p53 has been known as the “guardian of the genome” for many years with its direct roles in tumor suppression and apoptosis, the discovery and study of its cousin proteins p63 and p53 yielded a great amount of research. Many studies focus on the roles of p63 and p53 in skin development and cancers alike (Ryu et., 2018). p53 and its related protein p63 and p73 make up the p53 tumor protein family. While p53 is the commonly mutated gene in many human cancers, p63 is seldom mutated or deleted. However, many cancers show an over-expression of p63 (Inoune and Fry 2014). Previous studies have shown that the loss of p63 is associated with tumorigenesis and cancer progression. As a result, whether p63 acts a tumor suppressor or as an oncogene has been argued. The reason for this, is that variably expressed p63 isoforms (via alternative splicing) appear to have different functions that are both like and different from p53 (Inoune and Fry 2014). There are strong structural similarities between p53 and p63 which allow p63 to bind to conventional p53 components (Stindt et al,. 2014). However, p63 has a very distinct function which plays a pivotal role in skin and limb development (Lustig 2012). For example, p63 dependent processes range from epidermal development of linages, to epidermis differentiation, and basement membrane formation (Stindt et al., 2014). Nearly all human tumors possess inactivating mutations in tumor suppressing proteins such as p53 which is crucial for cell cycle checkpoints and apoptosis. The p63 protein is an essential protein for skin development, maintenance, and has six main isoforms (Rangel et al., 2014).

The TAp63 isoforms (α, β, γ) can bind to DNA via p53 response elements (REs) and induce gene activation for cell cycle arrest and apoptosis (Rangel et al.,

2014). It can also inhibit terminal cell differentiation (Rangel et al., 2014). The ΔNp63 isoforms (α, β, γ) can also bind to DNA via p53 REs while exerting a dominant effect on p53, p73, and p63. This happens via competition for DNA binding sites or by protein-protein interactions (Rangel et al., 2014). Many cancers express mutant p53 proteins without the wild type tumor suppressing activity via a single missense mutation resulting in a single amino acid change (Stindt et al., 2014). Cancerous cells with wild-type p53 are expected to be more susceptible to cytotoxicity than those with mutant p53. However, wild-type p53 has been shown to enhance the pro-survival functions and increase survival advantages of cells. Mutant p53 can interact via aggregation with other proteins such as p63, p73, MDM2, and even wild type p53 (Inoune and Fry 2014). The MDM2 protein is a negative regulator of p53 which is responsible for p53 degradation and may have a binding affinity to p63 (Rangel et al., 2014). Some of these proteins can acquire oncogenic functions and contribute to tumorigenesis (Rangel et al., 2014).

References

Geller, Alan C, & Annas, George D. (2003). Epidemiology of melanoma and nonmelanoma skin cancer. *Seminars in Oncology Nursing*, *19*(1), 2–11. https://doi.org/10.1053/sonu.2003.50000

Inoue, K., & Fry, E. A. (2014). Alterations of p63 and p73 in human cancers. In Mutant p53 and MDM2 in Cancer (pp. 17-40). Springer Netherlands.

Laurikkala J. p63 regulates multiple signaling pathways required for ectodermal organogenesis and differentiation. Development. 2006;133(8):1553.

Lustig, D. (2012). Molecular Mechanisms of p63-Derived Ectodermal Dysplasia. A thesis submitted in conformity with the requirements for the degree of Master of Science Institute of Medical Science University of Toronto.

Pozniak CD. An anti-apoptotic role for the p53 family member, p73, during developmental neuron death. Science. 2000;289(5477):304.

Pozniak CD. p73 is required for survival and maintenance of CNS neurons. The Journal of neuroscience. 2002;22(22):9800

Rangel, Luciana P, Costa, Danielly CF, Vieira, Tuane CRG, & Silva, Jerson L. (2014).The aggregation of mutant p53 produces prion-like properties in cancer. *Prion*, *8*(1), 75–84.https://doi.org/10.4161/pri.27776

Ryu, T. H., Kye, H., Choi, J. E., Ahn, H. H., Kye, Y. C., & Seo, S. H. (2018). Features Causing Confusion between Basal Cell Carcinoma and Squamous Cell Carcinoma in Clinical Diagnosis. *Annals of dermatology*, *30*(1), 64–70. https://doi.org/10.5021/ad.2018.30.1.64

Stindt M H, Muller P A J, Ludwig R L, Kehrloesser S, Dötsch V, & K H Vousden. (2014). Functional interplay between MDM2, p63/p73 and mutant p53. Oncogene, Oncogene, 2014.

Su X. TAp63 prevents premature aging by promoting adult stem cell maintenance. Cell stem cell. 2009;5(1):64.

Yang A. p63 is essential for regenerative proliferation in limb, craniofacial and epithelial development. Nature. 1999;398(6729):714.

Yang A. p73-deficient mice have neurological, pheromonal and inflammatory defects but lack spontaneous tumours. Nature. 2000;404(6773):99.

CHAPTER TWO: THE p53, p63, p73 TRIO: AN EVOLUTIONARY FAMILLY AFFAIR OF HOMOLGY AND DIVERSE FUNCTIONLATY.

1. The p53, p63, MDM2 Protein Trio

1.1. Tumor Protein p53

The p53 protein is an important transcription factor involved in many physio-cellular pathways, especially that of programmed cell death (known as apoptosis), DNA repair, and cell cycle control (Oren 2003). This homo-tetrameric protein has three main functional and structural domains. These include the transactivation domain (TA) at the N-terminal which activates other genes, the DNA binding domain (DBD) which binds the promoter region of other p53 induced genes, and the oligomerization domain at the C-terminal which is responsible for the phosphorylation and acetylation of the p53 gene (Romer et al*.,* 2006). Recent studies have proposed that the formation of mutant p53 is strongly associated with some pathological effects including gain-of-function (GoF), loss-of-function (LoF), and domain-negative (DN) (Costa et al., 2016). These later proteomic effects play a pivotal role in tumorigenesis and cancer progression. p53 is lost in nearly half of all human cancers and tends to form aggregates such as amyloids just like the globular prion protein (PrP) (Rangel et al., 2014). This indicates that prion-like aggregation of mutant p53 could offer a novel mechanism of oncogenesis and that of p53 gain-of-function effects.

1.2 Transcription Factor p63

The p63 protein of the p53 family is structurally similar to p53 but with different functions. Some of these functions include epithelial tissue development,

tissue maintenance, and tumor suppression (Yang et al., 1998). The p63 gene codes for six isoforms (***Figure 1***) TAp63 (α, β, γ) and ΔNp63 (α, β, γ) (Yang and McKeon 2000). It is suggested that the full length TAp63 has similar functions to p53. Meanwhile, the truncated ΔNp63 which lacks the transactivation (TA) domain, acts as an inhibitor to p53, TAp63 and, TAp73 (Yang and McKeon 2000). However, the three ΔNp63 isoforms are structurally different and appear to have different transactivation abilities due to the presence or the absence of the Sterile Alpha Motif (SAM) and the Post-Sam domain at the C-terminal (Ghioni et al., 2005). Thus, it is commonly suggested that TAp63 is a tumor suppressor while the ΔNp63 is an oncogene. The p63 gene is responsible for the development and differentiation of normal skin, oral mucosa, and other tissues of ectodermal origin (Mills et al*.,* 1999). The TAp63 isoform is expressed during the initial stages of epithelial layer development, while the ΔNp63 isoform is later expressed in mature skin (epidermis) to inhibit the effects of the TAp63 isoforms (Koster and Roop 2004) and (Nguyen et al., 2006). Mutations of the p63 gene appear to have many apoptotic, proliferative, and senescence-like effects in cancerous tissues (Moll and Slade 2004). Because of the six different p63 isoforms, the roles, and effects of p63 on apoptosis are complex (Gressner et al., 2005). In many tissues, TAp63 induces apoptosis while the dominant ΔNp63 isoforms suppress many apoptotic pathways (Thurfjell et al., 2004). However, many studies have yielded unclear results concerning the functions and specific influences of the different p63 isoforms. The immunoreactivity of P63 is nuclear. The immunostaining of p63 has the diagnostic utility to prove squamous differentiation in poorly differentiated tumors, and to sort out malignant

versus benign proliferations in breast and prostate tumors (Kaufmann et al., 2001). p63 also identifies squamous differentiation in poorly differentiated carcinomas from various sites, particularly when expressed with cytokeratin 5/6 (CK5/6). p63+ and CK5/6+ are used by pathologist for poorly differentiated metastatic carcinomas that are likely to show squamous carcinoma primaries (Kaufmann et al., 2001). In normal tissues, p63 expression is restricted to epithelial cells of stratified epithelial such as skin, esophageal, cervical, tonsillar, and bladder tissues. In keratinocytes however, the expressed isoform is the ΔNp63 which presumably maintains epithelial cell proliferation at the stratum basale (Kaufmann et al., 2001).

1.3 Murine Double Minute 2 Protein (MDM2)

The Murine (Mouse) Double Minute 2 (MDM2) protein homolog, known also as the E3 ubiquitin-protein ligase MDM2, and is an important negative regulator of the tumor protein p53 in humans. MDM2 has two main functions. First, it functions as a ligase which recognizes and binds the N-terminal of p53. Second, it inhibits p53 transcriptional activation (Wade et al., 2006). MDM2 is an oncoprotein which induces ubiquitination, antagonizes p53, and may even carry p53-independent functions (Wienken et al., 2016). MDM2 is needed for organ and tissue development along with homeostasis. This is because unobstructed p53 activation leads to p53-overactivation-dependent cell death known as podoptosis (not apoptosis). MDM2 has an important mitogenic effect in wound healing after injury, where its inhibition interferes with the re-epithelization process (Ebrahim et al., 2015). MDM2 is a negative regulator of wild type p53 causing its degradation via ubiquitination. However, MDM2 cannot degrade mutant p53 due to the presence of

a phosphate group. MDM2 also shows different aggregation affinities when binding all three related proteins, both individually and collectively. Differences and mutations in the DNA binding domain of p53, p63, p73 play a crucial role in the binding affinity of MDM2 (Wienken et al., 2016). MDM2 plays an important role in the prognosis of many human cancers such as sarcomas, gliomas, melanomas, and carcinomas (Onel and Cordon-Cardo 2004). An autoregulatory feedback loop made of p53 and MDM2, strongly regulates p53 intracellular levels. Both p53 mutations and MDM2 overexpression can interrupt this loop and eventually be used as a negative prognostic indicator for cancer development (Javid et al., 2015). Even though MDM2 overexpression is common in many cancers, MDM2 can be both a positive or a negative indicator in tumors, thus still a controversial tumor differentiation biomarker (Onel and Cordon-Cardo 2004). In non-small cell lung cancer (NSCLC), the immunohistochemical detection of MDM2 favors MDM2 as a prognostic marker without the associated p53 expression (Ko et al., 2000). The overexpression in NSCLC gives a good prognosis without gene amplification, yet it can be correlated with high levels of MDM2 mRNA. Onel and Cordon-Cardo (2004) state that the prognostic value of MDM2 remains limited. This is due to the complexity of mechanisms involved in MDM2 overexpression in many tissues as well as the different physiological pathways regulating the MDM2 activity.

2. Functional Interplay

2.1. The Functions of the p53 and p63 Isoforms in Cancer

Recent oncology studies have shown that the expression of different p53 isoforms in different patterns may play a role in the regulation of normal and cancerous cells. The p53 genes encodes for 12 isoforms (SeJin and Seong, ,2016). These isoforms are expressed in normal cells via alternative translational initiation, alternative splicing, and alternative promoters. Research has also shown that the presence of mutant p53 aggregates may be linked to tumor pathogenesis because of the loss-of function (LoF), gain-of function (GoF), and the dominant-negative (DN) (SeJin and Seong, 2016). Many efforts have been made to single out correlations between the different expressed p53 isoforms (at the protein and the mRNA levels) and various cancers. studies such as Hofstetter et al. (2011) used different cell lines to study the p53 isoforms and their expression. These cells range from colorectal adenomas, mucinous and serous ovarian cancers, breast cancer, to squamous cell carcinomas of the head and neck (SCCHN) just to name a few (Boldrup and Bourdon, 2007). Fujita *et al.,* (2009) showed that the ratio of p53β to Δ133p53α can be used to predict the progression of a colorectal adenoma to a carcinoma. The expression of Δ40p53α was found to improve recurrence-free survival rates in mucinous ovarian cancer (Hofstetter et al., 2011). Furthermore, SCCHNs showed elevated levels of the p53β isoform (Boldrup and Bourdon, 2007). ***Figure 1,*** from the meta-analysis by SeJin and Seong (2016), summarizes the expression pattern of the p53 isoforms in different cancers. Many studies focused

on the central core domain of p53 because it is considered as a hot spot for nearly all genetic mutations such as R248Q. This later p53 mutant appears to self-aggregate more than wild type p53 and can seed further aggregation (Bom et al., 2012). SeJin and Seong (2016) state that p53 aggregation might be partially due to a decrease in the thermodynamic stability in the mutant protein's conformation. Additionally, p53 aggregates can further co-aggregate with wildtype p53 and cause cytotoxic effects on cells (Bom et al., 2012).

Cancer	Isoform	Remarks
Colorectal cancer	p53β, Δ133p53α	p53β/Δ133p53α expression ratio could allow cancer progression from colorectal adenoma to carcinoma.
Renal cell carcinoma (RCC)	p53β	p53β overexpression in tumors might play an important role in tumor stages, and could be a new predictor of cancer.
Mucinous ovarian cancer	Δ40p53α	Overexpression in the mucinous cancer sample more than normal ovarian tissue and high expression of Δ40p53α is a good predictor of improved recurrence-free survival.
Serous ovarian cancer	Δ133p53α	Higher disease-free survival and overall survival in mutant p53 advanced serous ovarian carcinoma patients.
	Δ40p53α	Higher disease-free survival and overall survival in WT p53 advanced serous ovarian carcinoma patients.
Breast cancer	p53γ	Bearing both mutant p53and p53 γ has a good prognosis as good as WT53.
	p53α, p53β, p53γ	Detection p53α, p53β, p53γ from only normal breast tissue.
	Δ133p53	Detected most of primary breast tumor.
Cholangiocarcinoma	p53α, Δ133p53	High expression ratio of p53 α/ Δ133p53 is associated with a shortened overall survival.
Acute myeloid leukemia (AML)	p53β, p53γ	Increased expression relies on chemotherapy.
Head and neck tumors (SCCHN)	p53β	p53β was detected in the majority of samples with the exclusion of Δp53 isoforms.
Melanoma	p53β, Δ40p53	Expressed at the mRNA level in the majority of melanoma cell lines, but were absent or undetectable in fibroblasts and melanocytes, suggesting that they could play a role in melanoma development.

Figure 1: p53 isoform expression and distribution in various cancers (SeJin and Seong 2016).

p53 is suspected as a "seed" for co-aggregation with other homologs such as p63 and p73 (Xu et al., 2011). Other *in vivo* studies demonstrated the accumulation of p53 aggregates using a fibrillar specific antibody (OC) or an amyloid oligomer specific antibody (A11) in breast cancer and basal cell carcinoma (BCC) FFPE

tissue biopsies (SeJin and Seong 2016). ***Figure 2*** shows the independent research that is geared toward p53 aggregation. Currently, cancer is being considered as an aggregation disease (Bom et al., 2012). During malignancy proteins are uncontrollably expressed with conformational changes. It has been demonstrated that the conformation of the p53 DNA-binding domain (DBD) is unstable (Stindt et al., 2014). Mutations such as R175H, R249S, and R273H additionally destabilize the DBD in p53. Thus, high percentages of these mutant proteins are unfolded and thus inactive (Switch laboratory “Cancer as an aggregation disease,” 2014). These mutants are found in about 30% of the documented clinical cases and are named “structural” mutants. Furthermore, the gain-of-function (GoF) and the dominant-negative (DN) activity of these structural mutants increase their aggregation tendency (Stindt et al., 2014). ***Figure 3*** Shows a native-PAGE of p53 transfected in SaOS-2 cells. Furthermore, the structure of the DNA-binding domain (DBD) of p53, p63, and p73 exhibit high homology along with aggregation sequences in the same structural protein motif which is highlighted in red (***Figure 5***). The R110P mutant p53 was shown to be co-expressed with p63 in SaOS-2 cells. ***Figure 6*** represents a 3D confocal microscopy image of a formed large p53 and p63 aggregates in the perinuclear region. This aggregation furthers explains p53’s oncogenic gain of function.

Domain	Status of protein	In vitro/in vivo	Conditions	Remarks
TA	1–63 fragment	in vitro	Expose to acidic pH.	These aggregates were shown to be cytotoxic to human SH-SY5Y cells
DBD	R248Q	in vitro	Expose to 37°C and pH 7.2.	The R248Q mutant aggregates to a larger extent than wild-type p53C when incubated at pH 7.2.
	p53C (AA94–312)			
	R248Q	in vitro	Gentle denaturation by pressure or temperature.	Aggregates, R248Q and p53C, have a similar behavior when perturbed by pressure or high temperature.
	p53C			
	R248Q	in vivo	Breast cancer tissues expressing mutant or wild type.	There was a strong correlation between tumor aggressivity and p53 aggregation.
	G245S			
	H193L			
	R175H			
	R273H			
	Y234C			
	I195L			
	Wild Type			
	R175H	in vitro	Zinc-free protein (ApoDBD)	ApoDBD can initiate aggregation of zinc-bound DBD via a nucleation-growth process.
TET	R337H	in vitro	Expose at pH 4.0 and higher temperatures.	Higher propensity to form amyloid-like fibrils more than WTp53.
	G334V	in vitro	At physiological temperature and pH.	G334V peptide forms amyloid aggregates by a two-step process.
	Full length	in vitro	Expose in vitro induced aggregates into the cell.	Aggregates can penetrate cells using macropinocytosis and coaggregate with cellular p53.
	N-terminal truncated (AA93–393)			

DBD = DNA-binding domain, TAD = transcription activation domain, TET = tetramerization domain.

Figure 2: Independent research on the aggregation of p53.

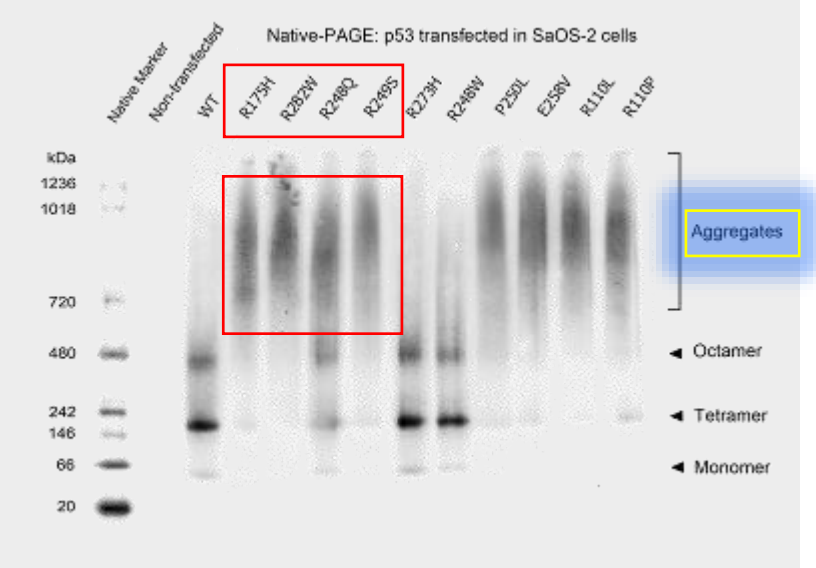

***Figure 4**: Native-PAGE: p53 transfected in SaCo-2 cells. (Switch Laboratory. Cancer as an aggregation disease, 2014).*

Figure 7 shows a schematic diagram of cell responses to DNA damage and the hypothesis of p53 aggregation. Under normal conditions, wildtype p53 tetramers are formed in response to cellular stress due to DNA damage. p53 then bind to the response elements and activate other tumor suppressing proteins such as p21. However, when a TP53 gene mutation occurs, it alters the expression of p53. This leads to the aggregation of expressed mutant p53, wildtype p53, and different isoforms.

2.2 The Functional Interplay of p53, p63, p73 and MDM2

During malignancy, Proteins are either uncontrollably over-expressed or structurally changed due to mutations causing changes in protein-protein interactions and functional activity (Stindt et al., 2014). Sometimes, it is still unclear whether the aggregation of tumor suppressors and oncogenes contribute to cancer progression and malignancy.

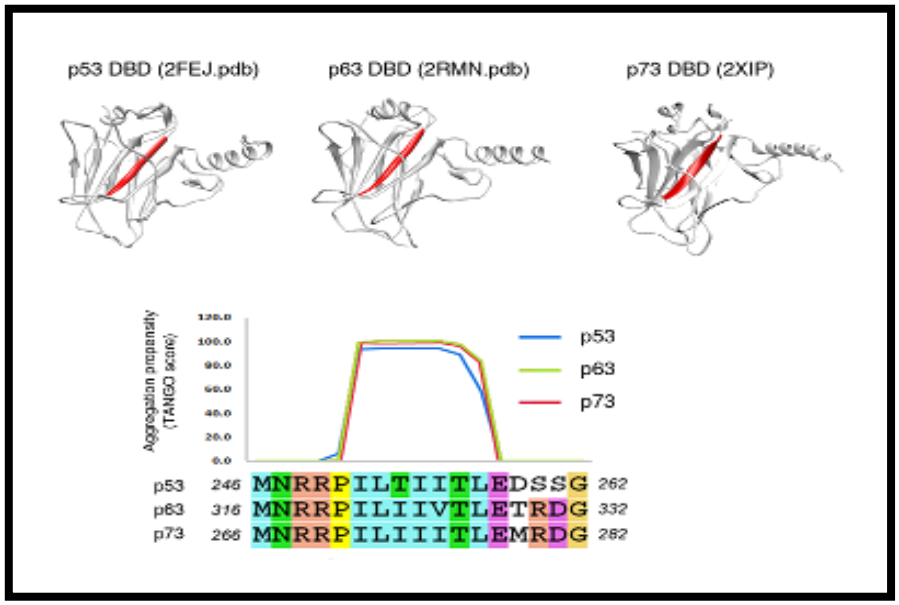

Figure 5*: The shared homology of the DBD of p53, p63, and p73. (Switch Laboratory, Cancer as an aggregation disease, 2014).*

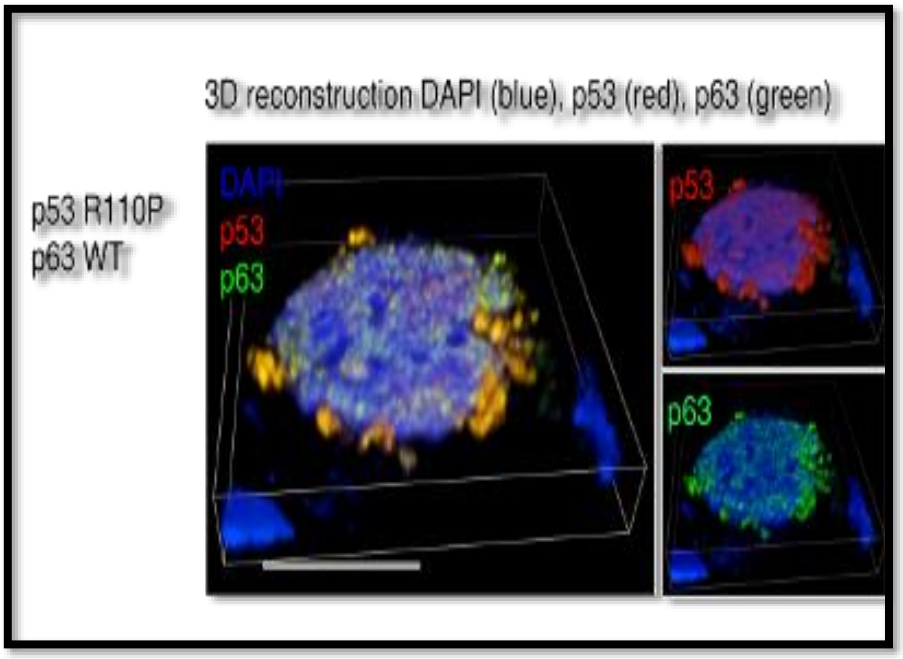

Figure 6*: p53-p63 aggregation formation in the perinuclear region of a SaOS-2 cell. (Switch Laboratory, Cancer as an aggregation disease, 2014).*

MDM2 is a key regulator of p53 function and can also bind to mutant p53 via the N-terminal binding region (Stindt *et al*., 2014). MDM2 also binds to nuclear p63 and facilitates its transport to the cytoplasm for degradation (Galli 2010). Studies by (Wang and Fersht, 2015) and (Stindt *et al.,* 2014) showed that there is a possible favored binding of MDM2 with mutant and wild type p53 rather than with p63 and that MDM2 reliefs the inhibition of p63 activity by binding mutant p53. ***Figure 6*** by Gannon (2012) shows the signaling pathway of p53, MDM2, and MDMX. Some studies showed that MDM2 inhibits p53 by interacting with the N-terminal transactivation (TA) domain. This leads to the suppression of downstream target genes associated with tumor suppression (Stindt et al., 2014). On the other hand, other studies showed that MDM2 destabilizes p53 via its E3 ligase activity.

Furthermore, p53 can also upregulate the expression of MDM2 by binding the p53 consensus sequence found on the MDM2 promoter region. Ryan *et al* (2001) has demonstrated that p53 is also able to maintain its own levels of expression via the upregulation of MDM2. This later pattern of interactions forms a negative feedback mechanism which maintains low levels of p53. p73 is another p53 family member. It is also involved in cell cycle regulation and apoptosis. Thus, considered a tumor suppressor as well (Harms and Chen, 2006). Unlike p53, MDM2 overexpression stabilizes p73 instead. However, many studies have shown inconsistent data on the effects of MDM2 on p63 transactivation, stability, and binding affinity (Lustig 2012).

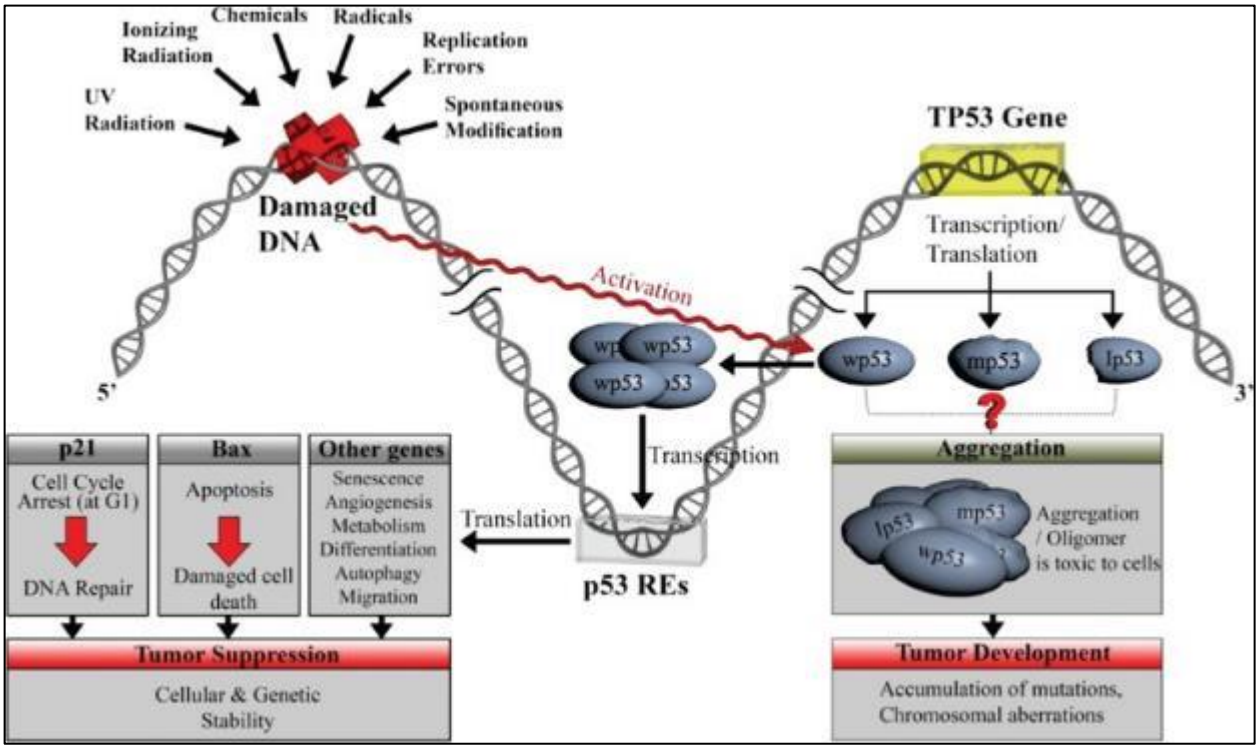

Figure 7: a schematic diagram of cell responses to DNA damage and p53 aggregation.

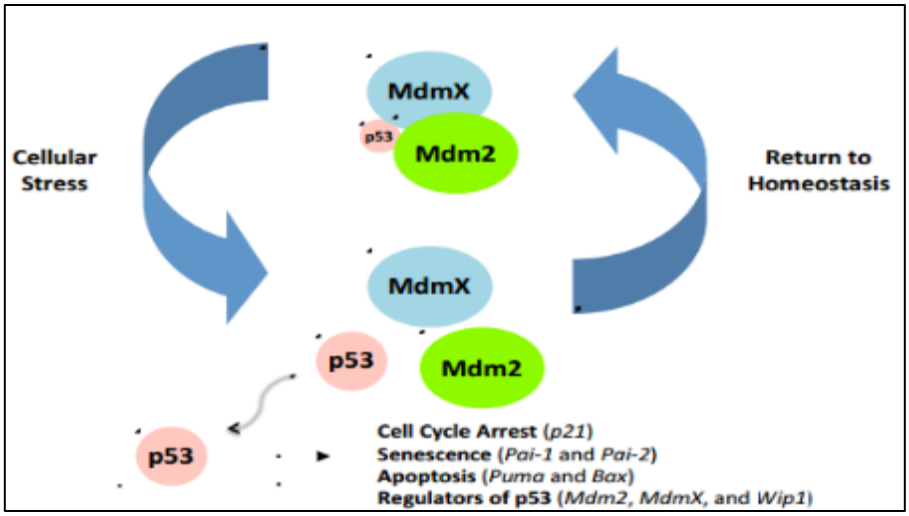

Figure 8: p53-MDM2-MDMX signaling pathway (Gannon, 2012)

Little (2001) states that MDM2 is unable to physically interact with either the Tap63 or ΔNp63. On the other hand, findings by (Lusting 2012) show that unlike p53, MDM2 cannot block the p63 transactivation of p21 which is one of the pathways for cell cycle arrest. This shows that many interactions between these proteins remain unclear. ***Figure 9*** by (Stindt et al., 2014) shows a representation of the binding effects of MDM2 on the inhibitory function of mutant p53 on p63 and p73.

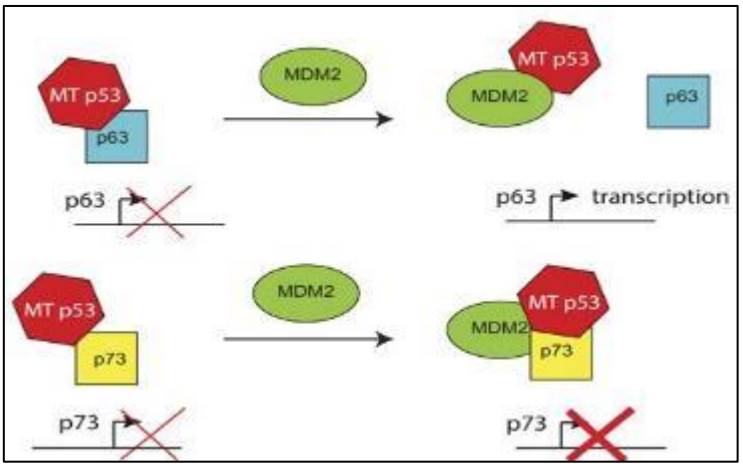

Figure 8: Representation of the binding effects of MDM2 on the inhibitory function of mutant p53, p63,and p73 (Stindt et al., 2014).

3. References

Boldrup L, Bourdon JC, Coates PJ, et al. Expression of p53 isoforms in squamous cell carcinoma of the head and neck. Eur J Cancer 2007; 43:617–23.

Bom APDA, Rangel LP, Costa DCF, et al. Mutant p53 aggregates into prion-like amyloid oligomers and fibrils implications for cancer. J Biol Chem 2012;287:28152–62.

Costa, D. C., de Oliveira, G. A., Cino, E. A., Soares, I. N., Rangel, L. P., & Silva, J. L. (2016). Aggregation and Prion-Like Properties of Misfolded Tumor Suppressors: Is Cancer a Prion Disease?. *Cold Spring Harbor perspectives in biology*, *8*(10), a023614. https://doi.org/10.1101/cshperspect.a023614

Ebrahim M, Mulay SR, Anders HJ, Thomasova D (November 2015). “MDM2 beyond cancer: podoptosis, development, inflammation, and tissue regeneration”. Histology and Histopathology. 30 (11): 1271–82.

Fujita K, Mondal AM, Horikawa I, et al. p53 isoforms Delta133p53 and p53beta are endogenous regulators of replicative cellular senescence. Nat Cell Biol 2009.

Galli F. MDM2 and Fbw7 cooperate to induce p63 protein degradation following DNA damage and cell differentiation. J Cell Sci. 2010: 123: 2423.

Gannon, H. S. (2012). Mdm2-p53 Signaling in Tissue Homeostasis and the DNA Damage Response: A Dissertation.

Ghioni, P., D’Alessandra, Y., Mansueto, G., Jaffray, E., Hay, R. T., La Mantia, G. and Guerrini, L. (2005). “The protein stability and transcriptional activity of p63 alpha are regulated by SUMO-1 conjugation.” Cell Cycle 4(1): 183-90.

Gressner, O., Schilling, T., Lorenz, K., Schulze Schleithoff, E., Koch, A., Schulze-Bergkamen, H., Maria Lena, A., Candi, E., Terrinoni, A., Valeria Catani, M., Oren, M., Melino, G., Krammer, P. H., Stremmel, W. and Muller, M. (2005). “Tap63alpha induces apoptosis by activating signaling via death receptors and mitochondria.” Embo J 24(13): 2458-71.

Harms, K. L., & Chen, X. (2006). P19ras brings a new twist to the regulation of p73

Hofstetter G, Berger A, Schuster E, et al. D133p53 is an independent prognostic marker in p53 mutant advanced serous ovarian cancer. Brit J Cancer

2011;105:1593–9.

Javid, J., Mir, R., Julka, P., Ray, K., & Saxena, C. (2015). Association of p53 and mdm2 in the development and progression of non-small cell lung cancer. Tumor Biology, 36(7), 5425-5432.

Kaufmann, O., Fietze, E., Mengs, J., & Dietel, M. (2001). Value of p63 and cytokeratin 5/6 as immunohistochemical markers for the differential diagnosis of poorly differentiated and undifferentiated carcinomas. American Journal of Clinical Pathology, 116(6), 823-30.

Ko, J.-L., Cheng, Y.-W., Chang, S.-L., Su, J.-M., Chen, C.-Y. and Lee, H. (2000), MDM2 mRNA expression is a favorable prognostic factor in non-small-cell lung cancer. Int. J. Cancer, 89: 265–270.

Koster, M. I. and Roop, D. R. (2004). “The role of p63 in development and differentiation of the epidermis.” J Dermatol Sci 34(1): 3-9.

Laurikkala J. p63 regulates multiple signaling pathways required for ectodermal organogenesis and differentiation. Development. 2006;133(8):1553.

Little NA. Hdmx and Mdm2 can repress transcription activation by p53 but not by p63.Oncogene. 2001;20:457.

Lustig, D. (2012). Molecular Mechanisms of p63-Derived Ectodermal Dysplasia: A Dissertation.

Mills, A. A., Zheng, B., Wang, X. J., Vogel, H., Roop, D. R. and Bradley, A. (1999). “p63 is a p53 homologue required for limb and epidermal morphogenesis.” Nature 398(6729): 708-13.

Moll, U. M. and Slade, N. (2004). “p63 and p73: roles in development and tumor formation.” Mol Cancer Res 2(7): 371-86.

Nguyen, B. C., Lefort, K., Mandinova, A., Antonini, D., Devgan, V., Della Gatta, G., Koster, M. I., Zhang, Z., Wang, J., Tommasi di Vignano, A., Kitajewski, J., Chiorino, G., Roop, D. R., Missero, C. and Dotto, G. P. (2006). “Cross-regulation between Notch and p63 in keratinocyte commitment to differentiation.” Genes Dev 20(8): 1028-42

Onel, K., & Cordon-Cardo, C. (2004). MDM2 and prognosis. Molecular

Cancer Research: MCR, 2(1), 1-8 Oren, M. (2003). “Decision making by p53: life, death and cancer.” Cell Death Differ 10(4): 431-42.

Pozniak CD. An anti-apoptotic role for the p53 family member, p73, during developmental neuron death. Science. 2000;289(5477):304.

Pozniak CD. p73 is required for survival and maintenance of CNS neurons. The Journal of neuroscience. 2002;22(22):9800.

Rangel, Luciana P, Costa, Danielly CF, Vieira, Tuane CRG, & Silva, Jerson L. (2014). The aggregation of mutant p53 produces prion-like properties in cancer. *Prion*, *8*(1), 75–84. https://doi.org/10.4161/pri.27776

Romer, L., Klein, C., Dehner, A., Kessler, H. and Buchner, J. (2006). “p53–a natural cancer killer: structural insights and therapeutic concepts.” Angew Chem Int Ed Engl 45(39): 6440-60.

Ryan KM, Phillips AC, Vousden KH. Regulation and function of the p53 tumor suppressor protein. Curr Opin Cell Biol. 2001;13(3):332-7.

SeJin K, Seong S. A. An. Role of p53 Isoforms and Aggregations in Cancer. Medicine, vol. 95, no. 26, 2016, pp. 1

Stindt M H, Muller P A J, Ludwig R L, Kehrloesser S, Dötsch V, & K H Vousden. (2014). Functional interplay between MDM2, p63/p73 and mutant p53. Oncogene, Oncogene, 2014.

Su X. TAp63 prevents premature aging by promoting adult stem cell maintenance. Cell stem cell. 2009;5(1):64.

Thurfjell, N., Coates, P. J., Uusitalo, T., Mahani, D., Dabelsteen, E., Dahlqvist, A., Sjostrom, B., Roos, G. and Nylander, K. (2004). “Complex p63 mRNA isoform expression patterns in squamous cell carcinoma of the head and neck.” Int J Oncology 25(1): 27-35.

Truong AB. p63 regulates proliferation and differentiation of developmentally mature keratinocytes. Genes development. 2006;20(22):3185.

Wade M, Wong ET, Tang M, Stommel JM, Wahl GM (November 2006). “Hdmx modulates the outcome of p53 activation in human tumor cells”. The Journal of Biological Chemistry. 281 (44): 33036–44

Wang, G., & Fersht, A. (2015). Propagation of aggregated p53: Cross-reaction and

coaggregation vs. seeding. Proceedings of the National Academy of Sciences of the United States of America, 112(8), 2443-8.

Wienken M, Dickmanns A, Nemajerova A, Kramer D, Najafova Z, Weiss M, Karpiuk O, Kassem M, Zhang Y, Lozano G, Johnsen SA, Moll UM, Zhang X, Dobbelstein M (January 2016). “MDM2 Associates with Polycomb Repressor Complex 2 and Enhances Stemness-Promoting Chromatin Modifications Independent of p53”. Molecular Cell. 61 (1): 68–83.

Xu J, Reumers J, Couceiro JR, et al. Gain of function of mutant p53 by coaggregation with multiple tumor suppressors. Nat Chem Biol 2011; 7:285–95.Yang A. p63 is essential for regenerative proliferation in limb, craniofacial and epithelial development. Nature. 1999;398(6729):714.

Yang A. p73-deficient mice have neurological, pheromonal and inflammatory defects but lack spontaneous tumours. Nature. 2000;404(6773):99.

Yang, A. and McKeon, F. (2000). “P63 and P73: P53 mimics, menaces and more.” Nat Rev Mol Cell Biol 1(3): 199-207.

Yang, A., Kaghad, M., Wang, Y., Gillett, E., Fleming, M. D., Dotsch, V., Andrews, N. C., Caput, D. and McKeon, F. (1998). “p63, a p53 homolog at 3q2729, encodes multiple products with transactivating, death-inducing, and dominant-negative activities.” Mol Cell 2(3): 305-16.

CHAPTER 3: *IMAGEJ* AND QuPath DIGITAL SEMI-QUANTIFICATION OF THE IMMUNOHICTOCHEMICAL EXPRESSION OF TP53, TP63, AND MDM2 IN SKIN BASAL CELL AND SQUAMOUS CELL CARCINOMAS.

1. Abstract:

Objective: The objective of this study was to evaluate and characterize the pattern of p53, p63, and MDM2 tissue expression in 2 types of skin cancers through immunohistochemistry (IHC) via innovative image processing softwares such as ImageJ and QuPath. **Study Design**: Three cases of cutaneous cancers: one basal cell carcinoma (BCC) and two squamous cell carcinomas (SCCs) were included in this study. The cases were diagnosed and classified by a trained pathologist before digital pathology image processing. Multiple regions of interest (ROIs) were identified in all three cases and captured at different magnifications. For each case, every ROI was at the exact region of the slide for each protein stained. This was repeated for each cancer case. 13 ROIs for each protein in the BCC case (total of 39 ROIs), 14 ROIs for each protein in the SCC (HIV+) case (total of 42 ROIs), and 9 ROIs for each protein in the SCC case (a total of 27 ROIs). **Materials and Methods**: Formalin-Fixed Paraffin-Embedded biopsies were obtained from Heartland Pathology Consultants Edmond, OK USA. Immunohistochemical staining was carried out using monoclonal antibodies for p53, p63, and MDM2. The semi-quantification of positive stain percentages in each ROI was performed via manual thresholding and the IIHC profiler plugin, both features of the ImageJ (FIJI) image processing software. The nucleus to cytoplasm ration was determined in all cases using the most representative ROIs. This was achieved via QuPath, a software for

quantitative pathology. **Results and Conclusions**: Our results indicate that an increase in dysplasia and histological tumorous features such as tumor nests correlates with an increase in tissue expression of p63 and MDM2 but not p53. p53 was the least expressed protein in all three cases with weaker in intensity when present. P53 was strong in intensity in one specific region of the epidermis in the SCC. p63 exhibited strong and strict nuclear expression in all cases while MDM2 had strong immunoreactivity but was expressed both in the nucleus and cytoplasm of cells in all three cases. MDM2 also was expressed in the subdermal layer and connective tissue. p63 was highly significant in differentiating the three cancer cases (p-value = 0.0007) followed by p53 which was marginally significant (p-value = 0.086) while MDM2 was of no significance in differentiating the cancer cases (p-value = 0.718).

2. Introduction

The ability to have high resolution images and scans of whole tissue slides is critical to tumor identification, biomarker expression, and digital analytics. This emerging field of tissue image analysis is referred to as digital pathology (Bankhead et al., 2017) and (Hamilton et al., 2014). Digital pathology uses computer and software platforms to view digital images of tissue slides via whole slide images (WSIs) or regions of interest (ROIs) cropped from the WSIs (Williams et al., 2017). WSIs are usually obtained from high resolutions microscopes made specifically for digital pathology downstream quantification protocols (Pell et al., 2019). Current pathology professionals and researchers have a selection of working softwares to choose from, such as CellProfiler (Lamprecht et al., 2007), Icy (De Chaumont et al.,

2012), and Fiji which is an updated version of ImageJ (Schindelin et al., 2012). These softwares allow researchers to share their findings and analysis solutions in the form of plugins, scripts, pipelines, and workflows. This enhances the reproducibility of high content imaging results and research protocols respectively (Bankhead et al., 2017). The field of digital pathology continues to lack a standardized peer-accepted open and accessible software platform for image analysis (Satyanarayanan et al., 2013). This means, that without access to expensive commercial analytical platforms, users will have to resort to ineffective methods such as downsampling and cropping of images (Bankhead et al., 2017). This eventually allows them to apply general analysis tools to only a subset of imagery data. Thus, compromising reproducibility and causing high result variability (Tuomien et al., 2010) and (Marée et al., 2016).

Our project aims to use image analysis on semi-quantitative tissue morphological metrics of cancerous skin in key areas, such as the standardization of immunohistochemical stain interpretation, the assessment of tumor cellular characteristic, and the correlation of findings with that of pathologist's diagnostic findings. Image processing and analysis in digital pathology potentially provide better accuracy, more reproducible results, standardization, and the extraction of new information from both novel and existing features and software plugins. (Pell et al., 2019). A pathologist's assessment remains the golden standard in diagnostic pathology due to the experience of a trained eye. However, digital pathology helps complement such assessment and diagnoses, further improve prediction models, and perform functions outside manual capability (Pell et al., 2019). Quantification of

immunohistochemical tissues, circularity of cells and nuclei, and nucleus to cytoplasm ratios are one of the many metrics digital pathology help incorporate into clinical practice and trials (Koelzer et al., 2018). These latter methods provide quantifiable data about individual cells of interest and tissue components such as glands and tumor nests (Pell et al., 2019). *QuPath* and *ImageJ* (currently known as FIJI) are open source softwares which allow for digital pathology image analysis. These softwares are user friendly, allow *whole slide image*s (WSI) analysis including *regions of interest* (ROIs), and offer extendable solutions complementary to diagnoses by a pathologist. The image analysis methodology offers tumor identification and biomarker expression evaluation tools (Schindelin et al., 2012). It also allows the user to perform powerful batch processing, share new functionality algorithms, and analyze complex tissue images (Bankhead et al., 2017). Whole slide imaging can easily generate large 2D images or *z-stacks* where each plane may contain up to 40 GB of data. Manual scoring by a pathologist can be difficult and sometimes is not satisfactory for large-scale biomarkers studies. This is due to the need for reliable, accurate, reproducible analyses for tissue biomarkers and their selection for clinical trials. Lately, this has led to the development of new image processing softwares for whole slide pathology slides (Bankhead et al., 2017).

The QuPath software has been a user friendly and a great open-source software that addresses many said challenges facing image analysis. It is by far the first comprehensive open-source software geared toward whole slide image analysis and applications. QuPath is characterized by a functional cross-platform core that is multithreaded and has a tile-based whole slide viewer. This software

also offers new algorithms for powerful scripting functionality. The QuPath functionality has algorithms such as *tissue microarray* (TMA) analysis, whole tissue section analysis, cell detection and classification, feature computation, and survival analysis (Bankhead et al., 2017). One of the main advantages of QuPath and ImageJ is that users can add their own extensions based either on challenges they have faced or aims of their projects. Furthermore, one the key feature of this software is that it is an "*object*" based data model (Bankhead et al., 2017). In this case the word "object" refers to a region or a structure of interest within the image being analyzed. One can subsequently manipulate such object by either using *annotations* (e.g., drawings, symbols) or *automated segmentation commands* (e.g., detection and separation of individual cell or nuclei). These later functions allow a researcher to display any possible relationships between multiple image-objects using gigapixel images and object classifiers (Bankhead et al., 2017). One of the most applied examples of QuPath and ImageJ is the ability to evaluate the presence, localization, and the intensity of biomarkers' expression in IHC slides (Bankhead et al., 2017). These biomarkers are classic tools in the field of immunohistochemistry and pathology alike. They are typically detected using specific antibodies and chromogens (Bankhead et al., 2017). In addition to measuring biomarker expression, stain intensity, and cell morphology, QuPath and ImageJ have a built-in "cell segmentation algorithms" which can detect thousands of cells within a single whole slide image (WSI). This later classifies different cell types creating a comprehensive phenotypic cellular profile of the WSI or ROI (Bankhead

et al., 2017). This allows for the semi-quantitative map out the tissue section and the discovery of any subtle morphological features not visible by the naked eye.

p53 Immunohistochemistry in Pathology

The most common genetic alterations in human tumors are mutation of the TP53 tumor suppressing gene (Rangel et al., 2014). The resulting altered protein has an extended half-life and is detectable with IHC. One should also note that epigenetic changes can cause protein accumulation. The gene product is a nuclear protein; hence the stain is nuclear. One must also note that p53 is detected by immunohistochemical stains only if a mutation renders it stable. Nonetheless, the protein may not be functional. A mutation can also cause a physiological response to genetic damage to some pathways such as that of MDM2 controlling p53. Thus, the p53 immunostain is not an obligatory marker for a mutated gene (Pernick, N., MD. (2012). P53. Retrieved September 25, 2020, from http://www.pathologyoutlines.com/topic/stainsp53.html).

p63 Immunohistochemistry in Pathology

The p63 protein is consistently expressed in basal and stem cells of the stratified epithelium. Six different isoforms exist with unknown functions. Both p63 and p53 belong the second tier of antibodies required by a standard surgical pathology laboratory. Positive staining (normal) for p63 consists of the following tissues and tissue organs: 1) Breast’s myoepithelium (Am J Surg Pathol 2001;25:1054). 2) Gynecologic tract’s basal and parabasal cells of mature cervical, vaginal, and vulval squamous epithelium. 3) prostate basal cells. 4) Skin basal cells.

5) thymus epithelial cells. 6) Urothelium. 7) Lungs' bronchial reserve cells, metaplastic squamous bronchial epithelium of the lower strata. Tumor protein 63 can positively be diagnostic to diseases such squamous cell carcinoma and squamous component of adenosquamous carcinoma. The p63 stain is typically nuclear (Pernick, N., MD. (2012). P53. Retrieved September 25, 2020, from http://www.pathologyoutlines.com/topic/stainsp63.html).

MDM2 Immunohistochemistry in Pathology

Overexpressed in atypical lipomatous tumors such as dedifferentiated, and well differentiated liposarcomas (along with CDK4). Sarcomas like myxofibrosarcoma, leiomyosarcoma, and synovial sarcomas also show an MDM2/CDK4 overexpression (Pernick, N., MD, 2013. Retrieved September 25, 2020, from http://www.pathologyoutlines.com/topic/stainsmdm2.html). The MDM2 protein preferentially labels the perinuclear membrane in the granular layer of verrucous carcinoma tumor cells whereas it shows weak and sometimes strong cytoplasmic staining (Ouban et al., 2003).

Image Fundamentals

Digital images are made of pixels or picture elements where each pixel is a number. When image is displayed, the pixels' values are converted to squares of shades of gray (Bankhead et al., 2017). The goal of image analysis is to make sense of the converted values in a meaningful display pattern. Fluorescent images are additive and quantitative while brightfield images are subtractive and far less quantitative (Bankhead et al., 2017).

Object Annotation

An object refers to a pathological feature in the representative section of a specimen which is annotated which mean selected or drawn (Bankhead et al., 2017). This term can refer to a cell, a nucleus, or a selected region also referred to as a region of interest (ROI). Drawing regions of interest is one of the most frequently used features in digital pathology. ROI uses include the measurement of lengths and areas, the identification where of location where an analysis should be applied, and the selection of training regions for the classifier feature (Bankhead et al., 2017). The following picture (***Figure 1***) shows the type of annotations possible for an ROI selection.

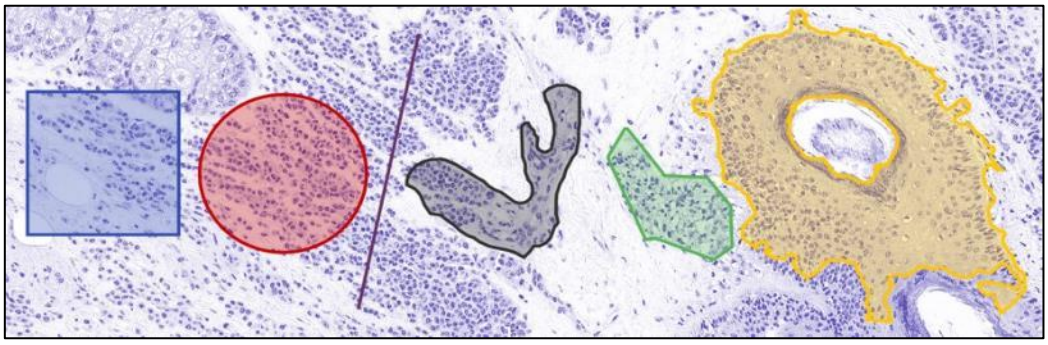

Figure 9*:* The figure shows multiple selected ROIs of different shapes (Bankhead et al., 2014).

Cell count

Counting cells is an especially important task for image analysis purposes and there are different ways to do it (Schindelin et al., 2012). Some methods are manual while others are automated. The automated method allows for simultaneous specifications about each cell such as diameter, area, pixel intensity, and nucleus to

cytoplasm ratio (Bankhead et al., 2017). Both the QuPath and imageJ platforms offer instructions to manually click on individual cell and count them (Bankhead et., 2017).

Object detection and classification.

The classification in this study is divided into positive and negative cells in reference to the stain in question (p53, p63, or MDM2). While manual counting can be very laborious and does not scale up to large number of objects (nuclei or cells). Softwares such QuPath and ImageJ have detection capabilities that are fast, accurate, and can yield reproducible results (Bankhead et al., 2017). Features such as object detection can help identify regions where the tumor is proliferating faster. For example, the number of tumor cells staining positive for Ki67, a marker for proliferation (Bankhead et al., 2017). Cells will also be classified as either negative or positive depending on the *score compartment of nucleus.* This score indicates how much DAB (3,3′-Diaminobenzidine) is in the nucleus (Schindelin et al., 2012). In other words, how brown do the nuclei look to the software. DAB is the chromogen used in immunohistochemistry. The DAB chromogen is attached to the secondary antibody specific to the protein of interest in IHC.

3. Methods

Skin Cancer Cases

A total of 3 Formalin-Fixed Paraffin-Embedded (FFPE) skin biopsies representing one BCC, one SCC, and one more SCC from an HIV positive patient were obtained from Heartland Pathology Consultants (HPC), Edmond Oklahoma.

The regions of interest (ROIs) make up the total samples For this study. The three cases will be graded per accepted and validated pathology diagnosing standards. The histology slides will be developed from pathology archival FFPE blocks. Hematoxylin and Eosin (H&E) staining will be performed to examine the morpho-pathology of the skin biopsies. Slides of the same biopsies will be stained for p63, p53, and MDM2 protein immunohistochemistry using the standard antibody protocols. Immunohistochemistry is a useful diagnostic tool for the differentiation of biomarkers' expression in different tissues.

Formalin-Fixed Paraffin-Embedded Tissue Biopsies

Archival formalin-fixed paraffin embedded (FFPE) tissue biopsies, along with their related diagnoses, represent an invaluable source for retrospective studies where prognosis and responses to treatment are well documented. The status of archival FFPE biopsies is that they serve an important source of material for many studies, including cancer proteomics. Nonetheless, proteomic studies face challenges such as diseases that progress slowly or malignancies with a larger time gap between recurrence and treatment. Furthermore, chemical reactions with formaldehyde and the harsh histology processing of the FFPE biopsies remain a hurdle for many analyses other than immunohistochemistry. Recent advances have been made in proteomic analysis protocols of FFPEs such as liquid-chromatography and mass spectrometry. Currently, for pathological diagnosis and differentiation, tissues are received from various medical facilities for pathological testing and analysis. The tissues are subsequently grossed, sectioned, and representative sections or whole biopsies are sent for processing in graded

formalin, alcohol, and xylene. The tissue sections are later embedded in paraffin. The frozen tissue blocks are mounted on a microtome, sectioned 5 to 10 μm in thickness, and then mounted on charged glass slides for either H/E staining or immunohistochemistry.

Grossing of Specimen

The skin cancerous biopsies differ in size, body location, patient medical history, and preoperative workup, particularly those of the head and neck. The grossing starts by describing the biopsies' shape, color, appearance, and measurement. Any abnormal changes located on the superior or inferior surfaces of the biopsy such as papules, macules, warts, or lesions should be thoroughly described and measured. One proceeds to inking the inferior margin of the specimen with any attached soft or adipose tissue, if inking is required for cancerous margin determination. Then one starts sectioning the specimen and describing the presence of hemorrhagic material, fluids, and the internal homogeneity of the specimen. One can either send the whole specimen or representative sections given the standard operating procedures. There are two general requirements to a skin biopsy grossing technique: representative and informative. The representative or adequate technique requires that the sample presented should show the most diagnostically valuable parts of the biopsy. The informative or definite technique requires the sample presented to have clear and unmistakable instructions for embedding and microtomy. When tissue biopsies are large, one should cut the biopsy into 3 mm thick sections with an area of approximately 20 mm x 30 mm if possible.

Tissue Fixation and Processing

Modern biopsy processing includes different auxiliary techniques requiring different modes of preservation. Fixation is the most universal technique of preservation. As a type of preservation, fixation plays two crucial roles. Besides its role of preserving the cellular structures, it also ensures the hardening of the specimen. The typical fixative for paraffin embedded tissues is neutral buffered formalin (NBF). This is equal to 4% paraformaldehyde in a buffer with added methanol to prevent the conversion of formaldehyde to formic acid. For an optimal histology protocol, a period of 24 to 48 hours is required for adequate tissue fixation. Inadequate fixation can lead to tissue dehydration which eventually results in hard, stiff, and breakable specimens while cutting with a microtome.

Using the tissue processor, the following steps are crucial for preparing tissue for embedding and microtomy:

1. 70% alcohol for 1 hour.
2. 95% ethanol (95% + 5% methanol).
3. First absolute ethanol for 1 hour.
4. Second absolute ethanol for 11/2 hour.
5. Third absolute ethanol 11/2 hour.
6. Fourth absolute ethanol for 2 hours.
7. First clearing agent (Xylene) for 1 hour.
8. Second first clearing agent (Xylene) for 1 hour.
9. First wax at 58^{o} C for 1 hour.
10. Second wax at 58^{o} C for 1 hour.

Paraffin Infiltration, Embedding, and Microtomy

During this step of tissue processing, tissues are dehydrated through graded alcohols and xylene to remove the water and allow the infiltration of paraffin into the tissue. The tissues are then embedded in paraffin blocks to be cut and stored for long periods of time. The most common waxes used are commercial paraffin waxes. These waxes normally made of straight carbon chain or n-alkanes between 20 to 40 carbons. The optimal histological use of the melting points of paraffin waxes range from 65^{o} C to 70^{o} C. For routine histology, paraffin melting temperature is usually between 56^{o} C to 58^{o} C. Increasing the temperature to 60^{o} to 65^{o} C range decreases viscosity which allows for better tissue infiltration. While the representative sections sent to be embedded are preferably 3mm thick, the slide-mounted cut sections range from 4 to 6 microns in thickness.

Immunohistochemistry

The IHC staining of all three cases was performed by NEO-Genomics (USA) using the proper antibodies for the p53, p63, and MDM2 special IHC staining.

Image Acquisition

Using a combination of CelSens software (Olympus Corporation of the Americas, Center Valley, PA, USA) and the IX-71 Olympus inverted fluorescent microscope with a DP 72 high-speed camera (Olympus Corporation of the Americas, Center Valley, PA, USA), and IHC stained FFPE samples from one BCC and two SCC cases. Objectives used include: 4x, 10x, 20x, and 40x. Images were acquired individually with the camera and processed via ImageJ and QuPath. 13

ROIs were captured from the BCC slides for each of the proteins p53, p63, and MDM2 totaling 39 ROIs. 14 ROIs were captured from the SCC (HIV+) slides for each of the three proteins totaling 42 ROIs. The ROIs all measured around 4128 x 2820 pixels.

Software Download

The *QuPath* and *ImageJ* (*FIJI*) source code, download, and documentation are available at the following webpage respectively:

https://qupath.readthedocs.io/en/latest/docs/intro/about.html

https://imagej.net/Fiji

ImageJ or (*FIJI*) is an open-source software which aims to improve and standardize the speed, objectivity, and reproducibility of digital pathology image analyses. These analyses are geared toward to the interpretation of biomarkers for whole slide images and regions of interest. Due to the lack of high-tech instrumentation for whole slide imaging, only regions of interests form each slide of each case will be considered for this study. *QuPath* has been developed for research purposes and applications by the Centre for Cancer Research & Cell Biology at Queen's University Belfast. This is part of a research project funded by Invest Northern Ireland and Cancer and Research UK. On the other hand, the imageJ software platform which is a property of the NIH and is also used to analyze the images of the histology tissue sections in this study. The research protocol consists of three main steps. The first step is the H&E staining of the selected skin pathologies. This is a standard step to evaluate the cancer pathological manifestations and to single

out areas of cellular interest. The second step is the immunohistochemical staining of p63, p53, and MDM2 of the three cancers using the standard antibody protocols. Routine diagnosis will be performed by a trained pathologist via visual inspection and scoring. The third step is to use a QuPath and ImageJ as tools to compare the three cases of skin cancers semi-quantitatively.

RGB Measurement

ImageJ analyzes the Red, Green, and Blue (RGB) channels of an image. Stain vectors are characterizations of how blue the hematoxylin is and how brown the DAB is. This lets the user know if the image is suitable for a semi-quantitative downstream analysis using ImageJ itself.

Manual Thresholding versus The IHC Profiler Plugin

In the field of anatomical pathology, immunohistochemistry (IHC) serves as the diagnostic and prognostic tool for the identification of diseases markers in tissues samples and biopsies (Varghese et al., 2014). These markers are crucial in the classification and grading of tumors and diseased tissues. In today's world of pathology, the intensity of the antibodies used in IHC staining of specific markers is manually judged and often times require more than one opinion of a pathologist (Varghese et al., 2014). The use of a plugin such as IHC Profiler from ImageJ facilitates and streamlines the assessment of antibody staining intensity in tissue sections. *IHC Profiler ImageJ* plug-in requires only very few steps to yield semi-quantifiable data about stain intensity resulting in the thresholding (segmentation) of only the positively stained cells in the image (Varghese et al., 2014). This gives a

binary view of the image where the stained tissue is black and white. For an 8-bit image the value of zero is assigned to a black pixel and the value of 255 is assigned to a very black pixel (Varghese et al., 2014). This means the positive nuclei and tissue will be black whereas the rest of the ROI is white where tissue, cell, and nuclei are unstained. The *IHC Profiler* plugin is able to do so by deconvoluting the IHC image's colors to 3-3'Diaminobenzadine (DAB) which is the actual stain for the biomarker in question and the hematoxylin the counter stain.

Interactive 3-D Surface Plot

The interactive 3-D surface Plot plugin from ImageJ is a tool used to provide three-dimensional characterization of the tissue samples and shows the homogeneity of tissue samples and also show areas of high conductivity (Schindelin et al., 2012).

4. Results

RGB Measurement

All the ROIs semi-quantified in this study had values of RGB that fell between 0 to 255 but not equal to neither 0 nor 255. This indicates that all images were suitable for all downstream analyses using imageJ including thresholding of the DAB stain and hematoxylin counterstain.

IHC semi-Quantification of p53, p63, and MDM2 in BCC and SCC cases

Finally, 9 ROIs were captured from the SCC slides for each of the proteins totaling 27 ROIs. This allowed us to semi-quantify the immunohistochemical tissue

expression of all three proteins in a total of 108 ROIs under different magnification. The semi-quantification of the DAB stain was achieved via *ImageJ* manual thresholding for the SCC (HIV+) case whereas the BCC and the SCC were semi-quantified via the IHC profiler plug-in in ImageJ also. We chose two different methods to show the optional methods to achieve such results. **Table 1** shows the average percentages of IHC DAB stain in every case for all three proteins.

	p53 % Stain	p63 % Stain	MDM2 % Stain
BCC	0.21	12.93	15.94
SCC (HIV+)	1.53	7.25	19.96
SCC	1.88	5.97	21.94

Table 1: Percent stain of p53, p63, MDM2 in all three skin cancers from all ROIs processed via *ImageJ* manual Thresholding and *ImageJ IHC Profiler*.

The results of the semi quantification of showed that p53 was the least expressed in all three cases. p53 was nearly absent in BBC and but was present in both SCC cases. MDM2 had the highest average percentage of positive staining and this is due to the act that MDM2 was diffusely positive in the nuclei, cells' cytoplasm, a subdermal tissue of in all cases. p63 stained positive in all cases butt higher in the basal cell carcinoma case.

IHC of p53, p63, and MDM2 in Basal Cell Carcinoma

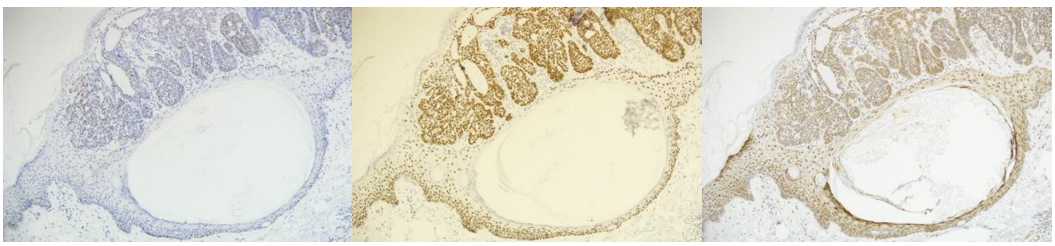

Figure 10: ROI# 2 at X100 magnification. Left p53, middle p63, right MDM2.

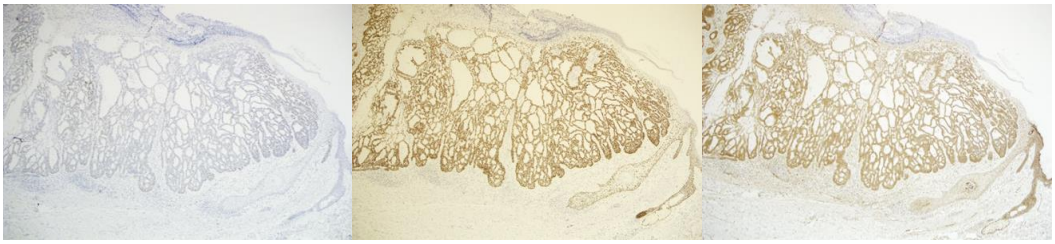

Figure 11: ROI # 11 at X40 magnification. Left p53, middle p63, right MDM2.

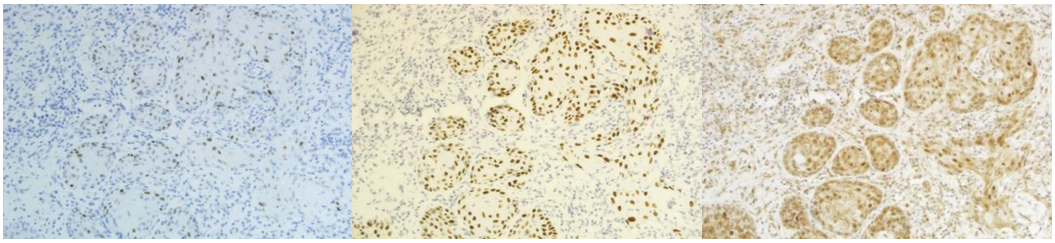

Figure 12: ROI # 13 at X200 magnification. Left p53, middle p63, right MDM2.

IHC of p53, p63, and MDM2 in Squamous Cell Carcinoma (HIV+)

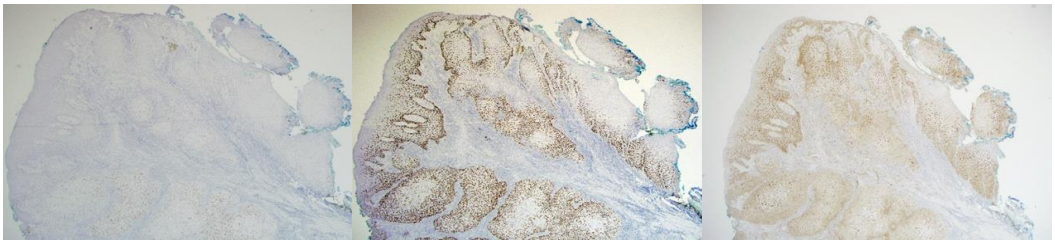

Figure 13: ROI #1 at X40 magnification. Left p53, middle p63, right MDM2.

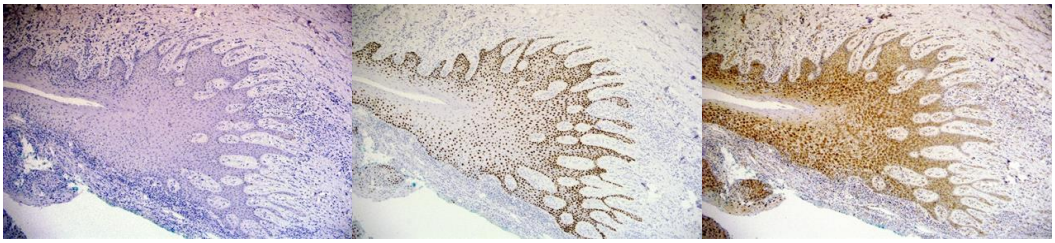

Figure 14: ROI #4 at X100 magnification. Left p53, middle p63, right MDM2.

Figure 15: ROI #7 at X200 magnification. Left p53, middle p63, right MDM2.

IHC of p53, p63, and MDM2 in Squamous Cell Carcinoma

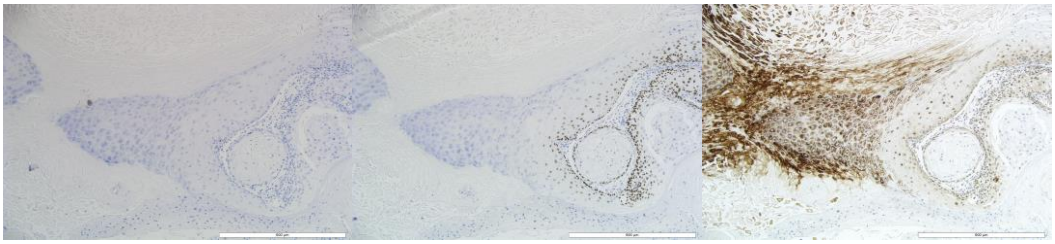

Figure 16: ROI #2 at X100 magnification. Left p53, middle p63, right MDM2.

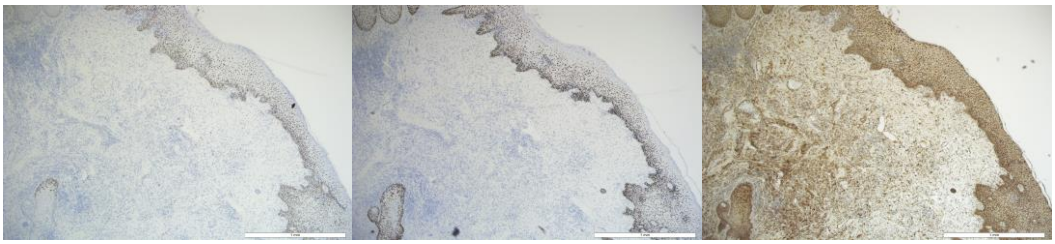

Figure 17: ROI #4 at X40 magnification. Left p53, middle p63, right MDM2.

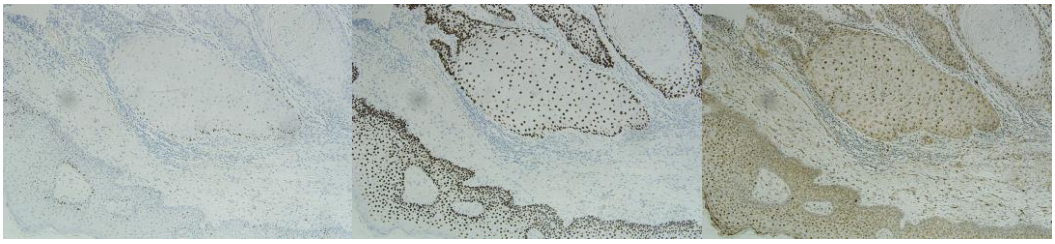

Figure 18: ROI #8 at X100 magnification. Left p53, middle p63, right MDM2.

Our results indicate that the tissue expression of p53 was weakly present in BCC and SCC (HIV+) tumor cells and was nearly absent in cells of the overlying healthy or unhealthy epidermis. However, a considerable part of the unhealthy SCC epidermis had strong p53 immunoreactivity whereas there was no tissue expression of p53 in the underlying dermal layer. Results also showed that p63's expression increased in the in the tumor cells and features of all cases. p63 epidermal expression was normal in the healthy epidermis of all cases. This means that p63 was absent in the outer most layers of the epidermis, the stratum granulosum

(granular layer) and the stratum corneum (cornified layer). p63 was nearly absent in the normal unaffected stroma of all cases. MDM2 immunoreactivity was decreased in BCC compared to SCC and SCC (HIV+). MDM2.

3D Surface Plot and Tissue Homogeneity Assessment

Three ROIs were chosen due to the presence of tumorous features that were assessed using the 3D-Surface-Plot ImageJ plugin. One ROI represent each of the different cases. Both squamous cell carcinoma cases show less tissue heterogeneity whereas the basal cell carcinoma case shows higher homogeneity. P63 was chose this analysis due to its strong stain intensity allowing for a better 3D surface plotting.

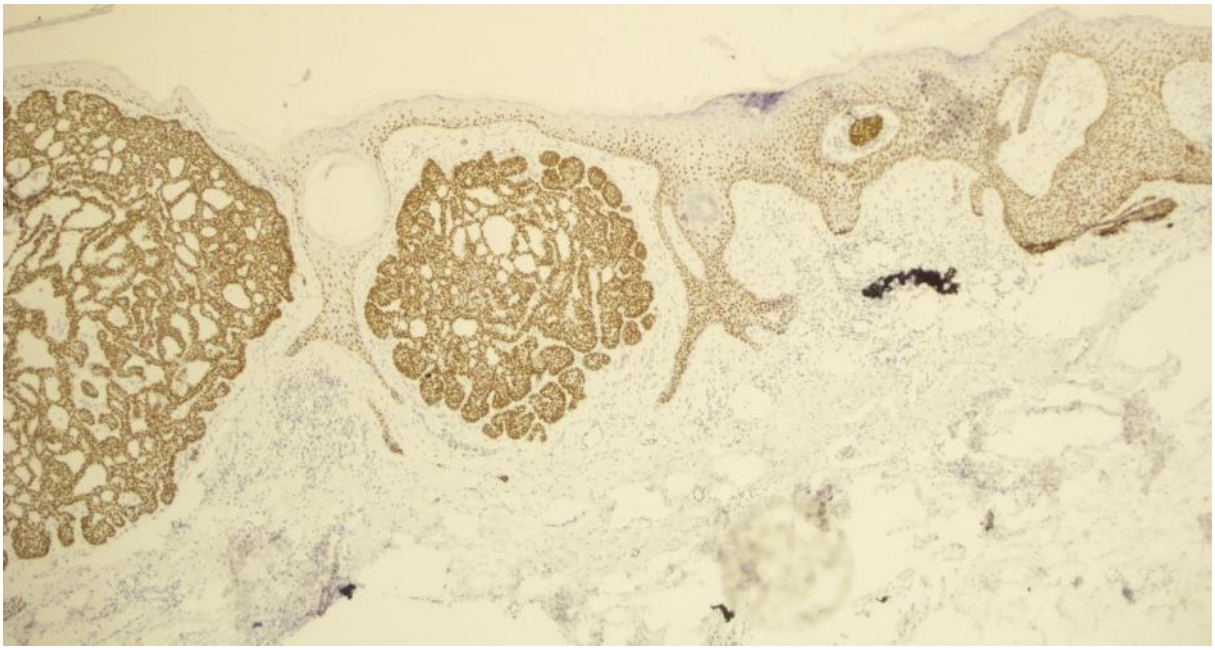

Figure 19: BCC ROI #4 at X40 magnification.

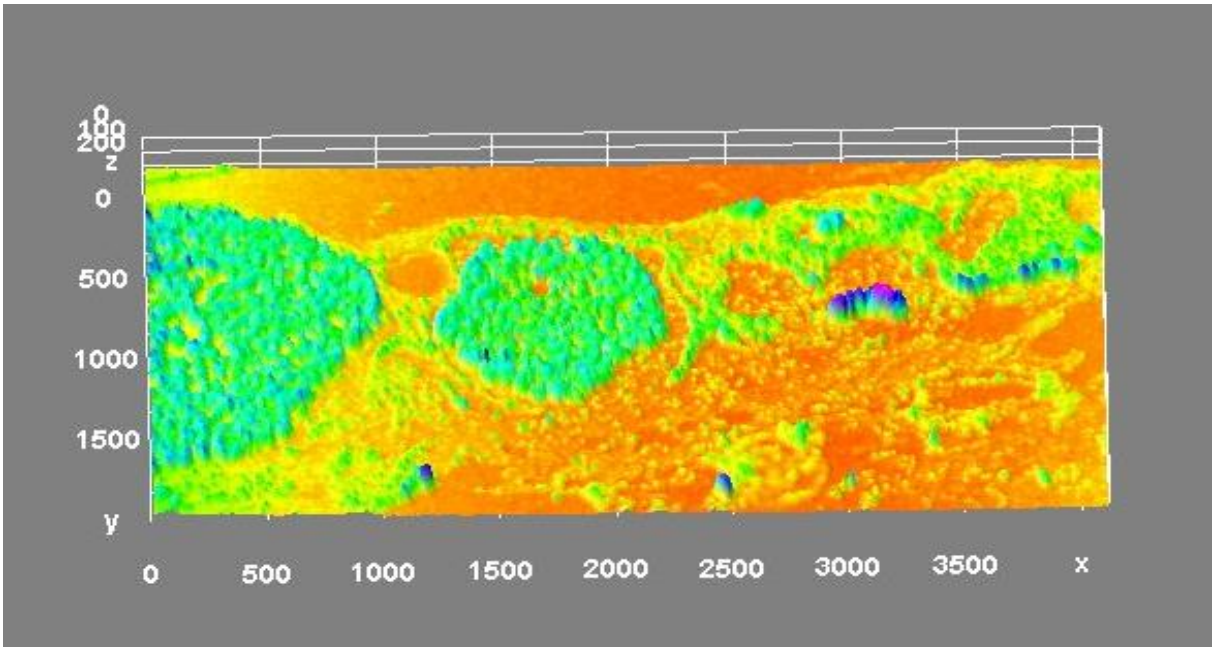

Figure 20: BCC ROI#4 shows a lesser color variation compared to both SCC and SCC (HIV+) ROIs.

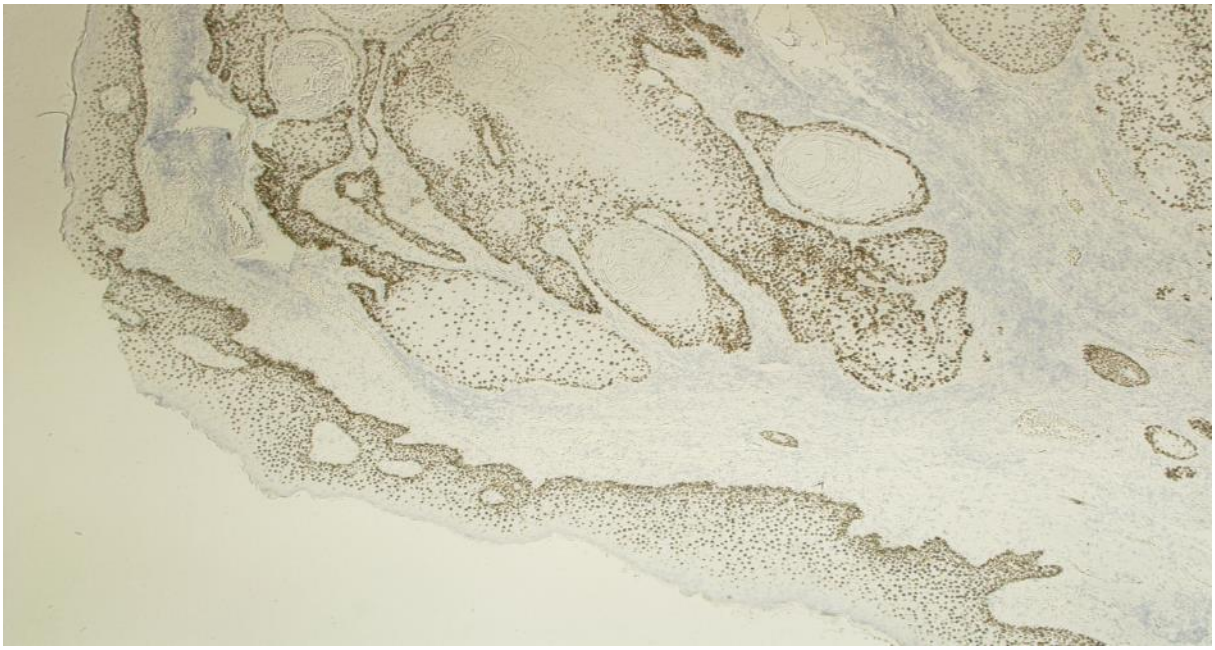

Figure 21: SCC p63 ROI #7 at X40 magnification.

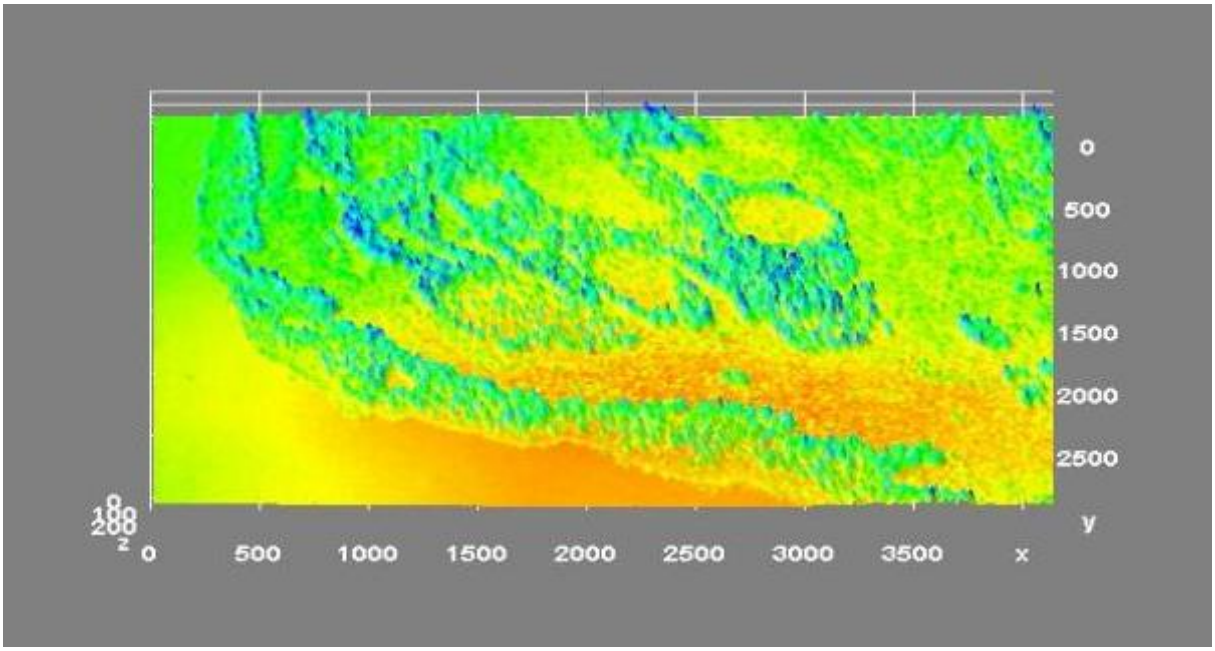

Figure 22: SCC p63 ROI #7 3D surface plot.

Figure 23: SCC HIV+ p63 ROI #4 at X100 magnification. The image shows the formation of possible lesional skin barrier (red arrow).

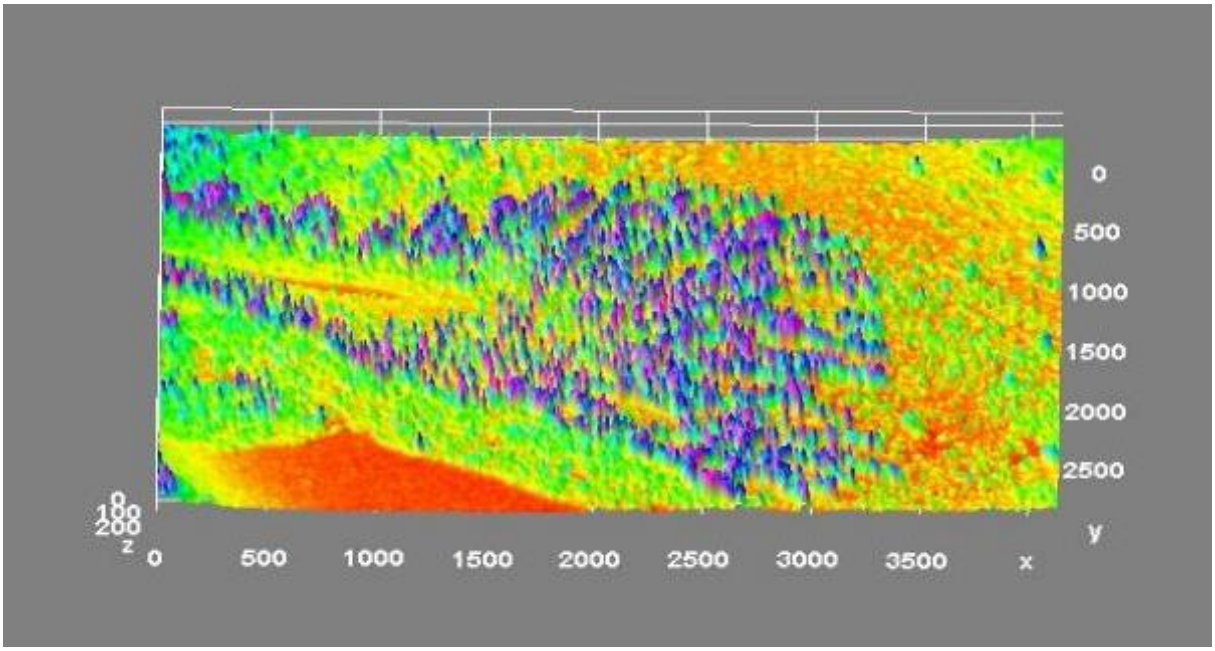

Figure 24: SCC HIV+ p63 ROI #4 shows 3D surface plot shows the most heterogeneity.

The 3D surface plot analysis shows the histological epidermal differentiation between cases. In all 3 cases, healthy regions of the skin are homogenous while in the tumorous skin regions are more heterogenous. The blue areas in the 3D surface plot diagrams are expressed with greater number of pixels and correspond to higher conductivity.

5. Discussion

During this study, using ImageJ and QuPath, we were able extract valuable semi-quantifiable IHC data of p63, MDM2 and p53, although p53 was hard protein to quantify. This is due to the strong and strict nuclear expression of p63, the diffuse nuclear and cytoplasmic MDM2 expression. p53 was hard to quantify in both BCC and SCC (HIV+) due to its weak immunoreactivity. Again, the methodology along with the results herein emphasize the important and complementary role of digital

pathology image processing platforms and software have in the field of pathology. p53 as a tumor suppressor is pivotal in the pathogenesis of many cutaneous cancers (Oh et al., 2020). The relevance of p53 and p53 mutations in the tumorigenesis of BCC and SCC is still not completely understood (Ishibashi et al., 2003) and (Campbell et al., 1993). The p63 protein is expressed as to isoforms. Research has shown that Tap63 is a tumor suppressing isoform whereas the ΔNp63 is an oncogenic isoform (Oh et al., 2020). One can speculate from the results herein and the finding of new studies whether the increased expression of p53, p63 and MDM2 in BCC and SCC is a consequence of the functional interplay between MDM2, wildtype p53, mutant p53, Tap63 and ΔNp63. The study by (Oh et la., 2020) factors in the formation of pyrimidine dimers and breaks DNA as a cause to such increase in tissue expression of these proteins. MDM2 is one of the major negative regulators of p53 (Oh et al., 2020). MDM2 does this either via the E3 ubiquitin ligase which recognizes the N-terminus of the trans-activation domain of p53 or via the inhibition of p53's transcription (Oh et al., 2020). Millon et al., (2001) showed a decrease in MDM2's expression in human head and neck SCC and that this decrease in expression was strongly associated with advanced stages of tumors and poor prognoses. The study by Oh et al. (2020) showed a decrease in MDM2 expression in BCC cells as opposed to the healthy overlying epidermis. To the best of our knowledge, this contradicts some of our finding where MDM2 was increased in expression and p53 was nearly absent in BCC. The ImageJ 3D surface plot-in shows significant variation in the tissue histology between BCC, SCC, and SCC (HIV+). According to Grammenandi et al., (2016), the 3D plot surface analysis

via ImageJ shows epidermal differentiation between the three cases. The SCC (HIV+) appears to be the most heterogenous which can indicate the formation of lipophilic tissue environment due to damaged cellular components. Grammenandi et al., (2016) suggest that the epidermal tissue differences are due to an increase in minerals such calcium anions and potassium and a decrease in low molecular weight antioxidants.

Here in we used advanced digital pathology software to extract valuable data from the IHC of p53, p63, and MDM2 in in BCC and SCC cancer cases. We found that both p53 and p63 can be used in tandem to differentiate between BCC and SCC in some cases where diagnosis can be difficult. We also found conflicting results from current research about the tissue expression of p53, p63, and MDM2 in BCC and SCC cutaneous cancers. We suggest that future research ought to focus exclusively on the IHC of p53 and p63 protein isoforms present in BCC and SCC skin cancers. This is due to the direct and pivotal roles these isoforms play in different skin layers. We also suggest that future projects can look at the presence of p53 and p63 amyloid aggregate in skin cancer due to the role they play in the gain-of-function (GoF) or the loss-of- functions of these proteins. We encountered few limitations in this study such a small sample (only three cases which make our findings comprehensive. Also, QuPath was not optimally compatible with the images used in this study because QuPath was originally designated for high resolution whole slide images (WSIs) which require specific digital pathology scanners.

6. References

Bankhead, P., Loughrey, M. B., Fernández, J. A., Dombrowski, Y., McArt, D. G., Dunne, P. D., … Hamilton, P. W. (2017). QuPath: Open-source software for digital pathology image analysis. Scientific Reports, 7, 16878.

Campbell C, Quinn AG, Angus B, Rees JL. The relation between p53 mutation and p53 immunostaining in non-melanoma skin cancer. Br J Dermatol 1993; 129: 235–241.

Fabrice De Chaumont, Stéphane Dallongeville, Nicolas Chenouard, Nicolas Hervé, Sorin Pop, Thomas Provoost, . . . Jean-Christophe Olivo-Marin. (2012). Icy: An open bioimage informatics platform for extended reproducible research. Nature Methods, 9(7), 690-6.

Grammenandi K, Kyriazi M, Katsarou-Katsari A, Papadopoulos O, Anastassopoulou I, Papaioannou GT, Sagriotis A, Rallis M, Maibach HI. Low-Molecular-Weight Hydrophilic and Lipophilic Antioxidants in Nonmelanoma Skin Carcinomas and Adjacent Normal-Looking Skin. Skin Pharmacol Physiol. 2016;29(6):324-331. doi: 10.1159/000453456. Epub 2017 Jan 19. PMID: 28099963.

Hamilton, Bankhead, Wang, Hutchinson, Kieran, Mcart, . . . Salto-Tellez. (2014). Digital pathology and image analysis in tissue biomarker research. Methods, 70(1), 59-73.

Ishibashi, Toyotaka, Kimura, Seisuke, Yamamoto, Taichi, Furukawa, Tomoyuki, Takata, Kei-ichi, Uchiyama, Yukinobu, Hashimoto, Junji, & Sakaguchi, Kengo. (2003). Rice UV-damaged DNA binding protein homologues are most abundant in proliferating tissues. *Gene*, *308*, 79–87. https://doi.org/10.1016/S0378-1119(03)00447-5

Koelzer VH, Sirinukunwattana K, Rittscher J, et al. Precision immunoprofiling by image analysis and artificial intelligence. Virchows Arch 2018. https://doi.org/10.1007/s00428-018-2485-z

Lamprecht, Michael R, Sabatini, David M, & Carpenter, Anne E. (2007). CellProfiler™: free, versatile software for automated biological image

analysis. *BioTechniques*, *42*(1), 71–75. https://doi.org/10.2144/000112257

Marée, R., Rollus, L., Stévens, B., Hoyoux, R., Louppe, G., Vandaele, R., … Wehenkel, L. (2016). Collaborative analysis of multi-gigapixel imaging data using Cytomine. Bioinformatics, 32(9), 1395–1401. http://doi.org/10.1093/bioinformatics/btw013

Millon, R, Muller, D, Schultz, I, Salvi, R, Ghnassia, J.P, Frebourg, T, Wasylyk, B, & Abecassis, J. (2001). Loss of MDM2 expression in human head and neck squamous cell carcinomas and clinical significance. *Oral Oncology*, *37*(8), 620–631. https://doi.org/10.1016/S1368-8375(00)00122-6

Oh, Shin-Taek, Stark, Alexandra, & Reichrath, Joerg. (2020). The p53 Signalling Pathway in Cutaneous Basal Cell Carcinoma: An Immunohistochemical Description. *Acta Dermato-Venereologica*, *100*(6), adv00098–2. https://doi.org/10.2340/00015555-3420

Ouban, A., Dellis, J., Salup, R., & Morgan, M. (2003). Immunohistochemical expression of Mdm2 and p53 in penile verrucous carcinoma. Annals of clinical and laboratory science, 33(1), 101–106.

Pell, Robert, Oien, Karin, Robinson, Max, Pitman, Helen, Rajpoot, Nasir, Rittscher, Jens, Snead, David, Verrill, Clare, Driskell, Owen J, Hall, Andy, James, Jacqueline, Jones, Louise J, Craig, Clare, Sloan, Philip, Thomas, Gareth J, Elliott, Philip, Cheang, Maggie, Rodriguez-Justo, Manuel, Rees, Gabrielle, … Morden, James. (2019). The use of digital pathology and image analysis in clinical trials. *The Journal of Pathology. Clinical Research*, *5*(2), 81–90. https://doi.org/10.1002/cjp2.127

Rangel, Luciana P, Costa, Danielly CF, Vieira, Tuane CRG, & Silva, Jerson L. (2014). The aggregation of mutant p53 produces prion-like properties in cancer. *Prion*, *8*(1), 75–84. https://doi.org/10.4161/pri.27776

Satyanarayanan, M., Goode, A., Gilbert, B., Harkes, J. & Jukic, D. OpenSlide: A vendor-neutral software foundation for digital pathology. J. Pathol. Inform. 4, 27 (2013).

Schindelin, Johannes, Arganda-Carreras, Ignacio, Frise, Erwin, Kaynig, Verena,

Longair, Mark, Pietzsch, Tobias, Preibisch, Stephan, Rueden, Curtis, Saalfeld, Stephan, Schmid, Benjamin, Tinevez, Jean-Yves, White, Daniel James, Hartenstein, Volker, Eliceiri, Kevin, Tomancak, Pavel, & Cardona, Albert. (2012).

Tuominen, V. J., Ruotoistenmäki, S., Viitanen, A., Jumppanen, M., & Isola, J. (2010). ImmunoRatio: a publicly available web application for quantitative image analysis of estrogen receptor (ER), progesterone receptor (PR), and Ki-67. Breast Cancer Research: BCR, 12(4), R56. http://doi.org/10.1186/bcr2615

Varghese, Frency, Bukhari, Amirali B, Malhotra, Renu, & De, Abhijit. (2014). IHC Profiler: An Open-Source Plugin for the Quantitative Evaluation and Automated Scoring of Immunohistochemistry Images of Human Tissue Samples. PloS One, 9(5), e96801–e96801. https://doi.org/10.1371/journal.pone.0096801

Williams BJ, Bottoms D, Treanor D. Future-proofing pathology: the case for clinical adoption of digital pathology. J Clin Pathol 2017; 70: 1010–1018

CHAPTER 4: A SOFTWARE ASSISTED PROTEOMIC MOLECULAR COMPARISON OF p53, p63, and MDM2.

1. Abstract: In recent years, protein aggregation has been at the center of proteomic and cancer research. Aggregation indicates the troubling instability of proteins. Identifying the molecular mechanisms dictating protein aggregation is crucial to understanding the pathogenesis of many diseases, the development of new diagnostic tests and drug therapeutics. **Objective:** The objective of this chapter was to summarize the data generated by three distinct web servers which use artificial intelligence and coding programs about the aggregation propensities of p53, p63, and MDM2, protein sequences, locations of amino acids and their hydrophobic and hydrophilic characteristics. **Study Design:** We have used three different web servers PATSA 2.0. AGGRESCAN, and FELLS to compare and contrast aggregation energies of p53, p63, and MDM2 and determine the location of hotspots in their protein sequences. **Materials and Methods:** We used the FASTA sequences of p53, p63, and MDM2 retrieved from the Protein Data Bank to run our aggregation stimulations. **Results and Conclusions:** Our results showed differences in the possible aggregation prone regions between PASTA 2.0 and AGGRESCAN. PASTA 2.0 predicted only one possible region of possible aggregation in p53, p63, and MDM2. Meanwhile AGGRESCAN predicted multiple hot spots most of which were clustered in the DBD of p53 and dispersed throughout multiple domains in p63. PASTA 2.0 also predicted that both p63 and MDM2 have 20 amyloids where p53 only has 6. The

FELLS webserver showed that p53 had the highest percentage of possible aggregation of 27.48% spanning 108 residues.

2. Introduction

Proteins misfolding, aggregation, and multiprotein complexes (MPCs) formation occur in numerous human degenerative diseases and are referred to as protein misfolding diseases (PMDs) (Dill and McCullum, 2012). These diseases are characterized by protein oligomers, protein fibrils, and mature fibrils which can occur both intra and extracellularly (Chiti and Dobson, 2006). One of the main models that explain the occurrence of these aggregates in their respective diseases is the prion model. This later model is based on the prion hypothesis which was pioneered by *Stanley Prusiner* in 1980s. Amyloid aggregates are caused directly by protein misfolding and recent research links p53 aggregation with the prion hypothesis (Walsh et al., 2014). An increasing number of diseases in different organ systems are associated with pathological deposition of protein aggregates (Aguzzi and O'connor, 2010). Diseases such as Alzheimer's disease and amyloidosis are the quintessence of such diseases (Aguzzi and O'connor, 2012). Nonetheless, with advancements in bottom-up proteomic testing, analytics, and artificial intelligence, research has shown that protein aggregation also occurs in the cytoplasm and the nucleus as opposed to the extracellular matrix only (Walsh et al., 2014). This indicates that amyloidosis encompasses many more diseases than previously thought of (Aguzzi and O'connor, 2012). ***Figure (1)*** by (Santos et al., 2020) summarizes how protein aggregation works against the normal physiological functions of proteins.

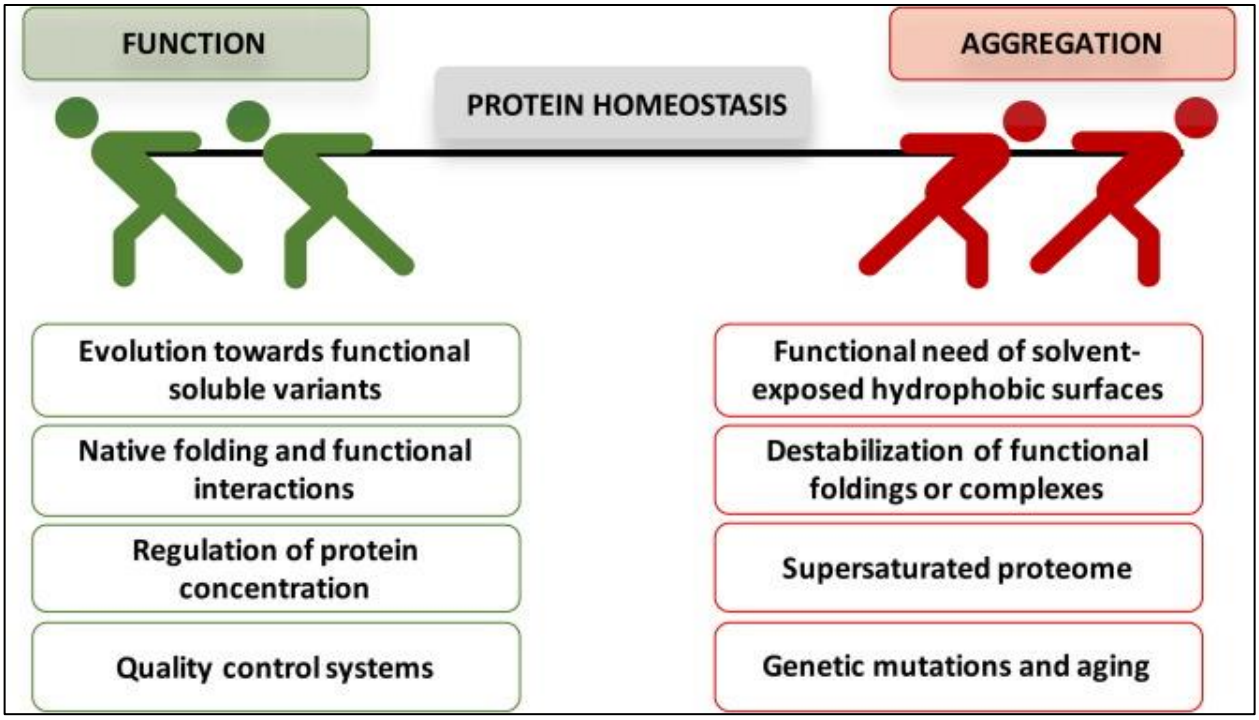

Figure 25: The innate competition between normal protein functions and non-functional aggregation (Santos et al., 2020).

The ability and tendency of protein to *self-aggregate* and *Co-aggregate* with other proteins or establish cross-amyloid molecular interactions between co-aggregated proteins, all depend on the stability of the amyloid "cross-beta" structure of the protein (Walsh et al., 2014). Herein, we used three distinct web servers PATSA 2.0, AGGRESCAN, and FELLS which use computational algorithms and bio-coding (using codes and programs for downstream biological analysis) and artificial intelligence to give a sequence based proteomic analysis of aggregation propensities and aggregation-prone regions (APRs) known as aggregation hot spots (Walsh et al., 2014). Amyloids are protein aggregates which fold together to form distinct shapes of many copies of the same protein known as fibrils (Walsh et al., 2014). Recent studies have shown that mutant p53 forms aggregates are

directly associated with gain-of-function (GoF), loss-of-function (LoF) and a dominant negative (DN) effect. ΔN63 isoforms do also show similar characteristics when exerting a negative dominant effect on all members of the p53 family. Rangel et al (2014) have proposed that these phenomena can be explained via a prion-like behavior of mutant p53. ***Figure (26)*** by Freed-Pastor and Prives (2012) shows the most frequent p53 mutations which occur mainly in the DBD of p53.

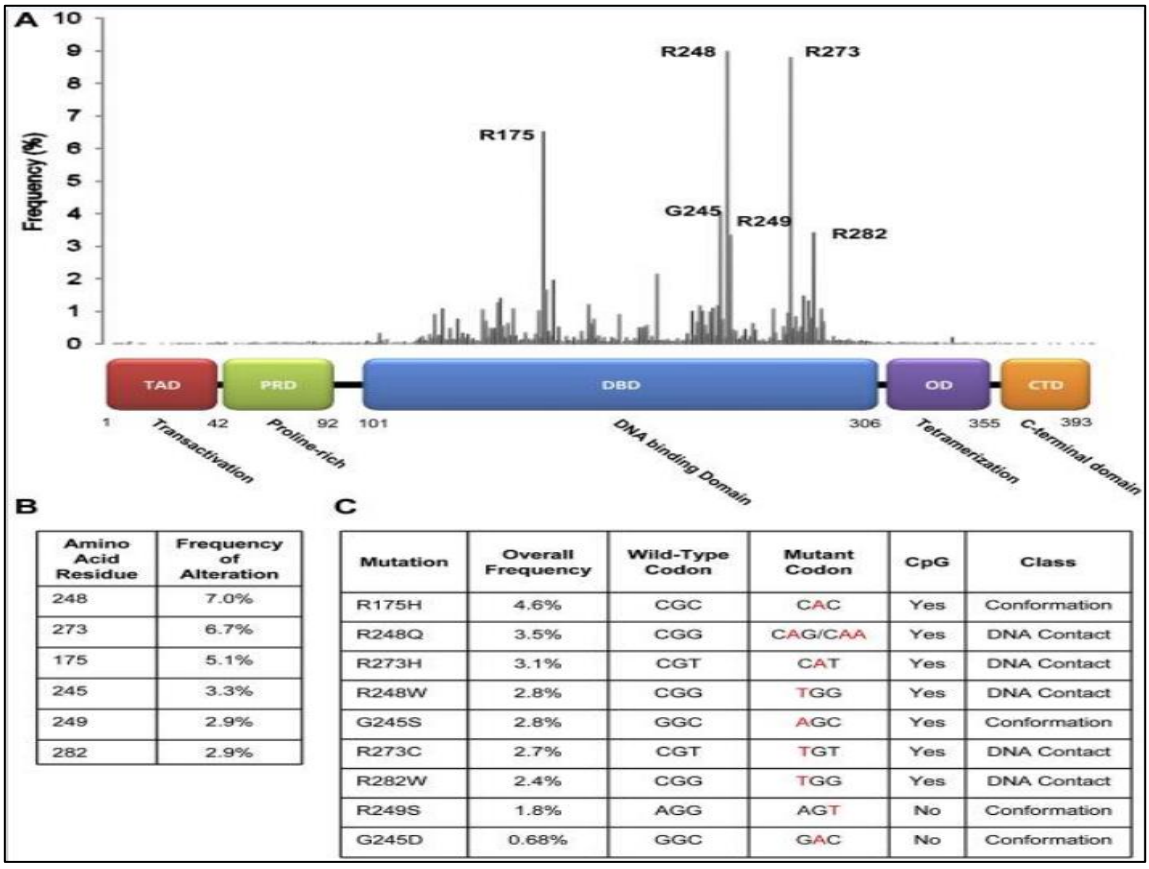

B

Amino Acid Residue	Frequency of Alteration
248	7.0%
273	6.7%
175	5.1%
245	3.3%
249	2.9%
282	2.9%

C

Mutation	Overall Frequency	Wild-Type Codon	Mutant Codon	CpG	Class
R175H	4.6%	CGC	CAC	Yes	Conformation
R248Q	3.5%	CGG	CAG/CAA	Yes	DNA Contact
R273H	3.1%	CGT	CAT	Yes	DNA Contact
R248W	2.8%	CGG	TGG	Yes	DNA Contact
G245S	2.8%	GGC	AGC	Yes	Conformation
R273C	2.7%	CGT	TGT	Yes	DNA Contact
R282W	2.4%	CGG	TGG	Yes	DNA Contact
R249S	1.8%	AGG	AGT	No	Conformation
G245D	0.68%	GGC	GAC	No	Conformation

Figure 26: p53 spectrum of mutations in human cancers. **(A)** Missense mutation data of p53 in human patients (N=19,262). **(B)** Six hot spots residues in p53 with their corresponding frequency of occurrence. **(C)** Most common missense mutations at hot spots p53 residues (Freed-Pastor and Prives, 2012).

The primary function of the ancestral p53 protein is to protect cells from DNA damage. This role has been conserved for over a billion years (Belyi et al., 2010). In the p53 family, p53 is the most divergent protein when compared to p63 and p73

which have a far more stable DBD (Belyi et al., 2010). This is due to the fat that p53 has taken on multiple tumor suppressing functions when protecting cells from DNA damage (Rangel et al., 2014). The evolutionary divergence of the p53 family protein is seen in their protein sequences. p53 is remarkably shorter (390 amino acids) than p63 (680 amino acids) and p73 (Belyi et al., 2010). p63 and p73 have all of the domains whereas p53 lacks some domains such as the Sterile Alpha Motif (SAM) domain. The p53 DBD only shares about 60% identify with those of p6 and p73 (Cino et al., 2016). The DNA binding domain (DBD) of p53 is innately unstable and is the cite for nearly all of the cancer causing p53 mutations (Cino et al., 2016). This is due to p53's DBD possessing amyloidogenic sequences and amyloid fibrils resulting in a loss-of-function (LoF) (Rangel et al., 2014).

3. Methods

Herein, we propose the use of three different protein aggregation webservers to characterize the aggregation propensities of p53, p63, and MDM2. The Prediction of Amyloid Structure Aggregation server (PASTA 2.0), Aggregation Scanner (AGGRESCAN) server, and the Fast Estimator of Latent Local Structure (FELLS) server are platforms that use computational algorithms based on existing and validated proteomic data in order to yield accurate stimulations about the protein aggregation energies along with the location of the probable aggregation hot spots in a protein sequence.

PASTA 2.0 Aggregation Web Server

The redesigned Prediction of Amyloid Structure Aggregation 2.0 (PASTA 2.0) software represents a versatile web server for the amino where protein propensities can be predicted and calculated from a simple genetic sequence input (preferably a FATSA file from UniProt or NCBI online protein data bases). The calculated energy functions by PASTA 2.0 shows the stability of the cross-beta amino acid pairing between different sequence stretches. The PASTA 2.0 server works best with FASTA type protein sequences of any database such as the PDB, UniProt, or NCBI databases. These protein amino acid sequences can be either copied and pasted from sites such as PDB and NCBI into the input window or downloaded from a saved file containing the protein sequence as shown in ***Figure (27)***. After entering the protein amino acid sequence, it is optional for the user to adjust the energy settings such as the top pairing energies and the energy threshold. Walsh et al., (2014) state that increasing sensitivity (TPR) will have a negative effect on specificity (FPR) of the stimulation and vice versa. The settings during this aggregation analysis of p53, p63, and MDM2 were kept on their default values.

AGGRESCAN Aggregation Web Server

AGGRESCAN is web server for predicting aggregation-prone regions in a protein sequence. It also analyzes the effect of mutations on the aggregation propensities of proteins and compares data between different sets (Conchillo-Sole et al., 2007). AGGRESCAN also uses FASTA protein sequences from the PDB, UniProt, or NCBI databases**.** ***Figure (28)*** shows the sequence input window of AGGRESCAN

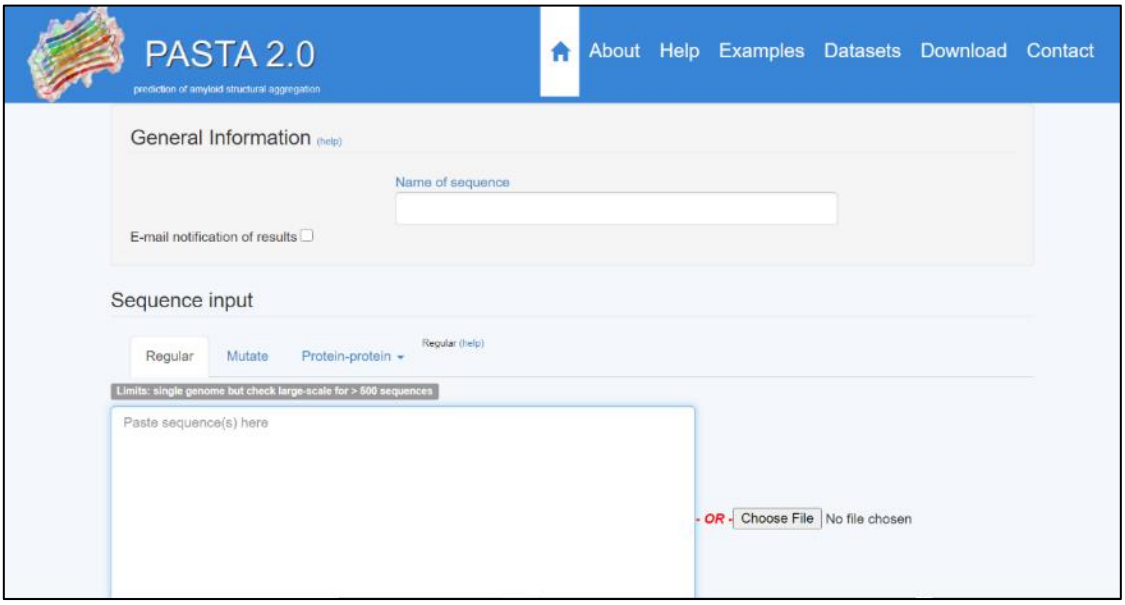

Figure 27: Screenshot of the PASTA 2.0 input window for protein sequences.

FELLS Aggregation Web Server.

The FELLS web server is geared toward visualizing structural features from protein sequences. The FELLS webserver yields aggregation and low complexity stimulations, disorder regions, and local residual propensities such regions of both hydrophobic and amphipathic clusters (Piovesan et al., 2017). The servers can be directly accessed via the following links:

PASTA 2.0: http://old.protein.bio.unipd.it/pasta2/

AGGRESCAN: http://bioinf.uab.es/aggrescan/

FELLS: http://old.protein.bio.unipd.it/fells/help

All of the protein sequences use in our study are in FASTA format and were retrieved from the UniProt database.

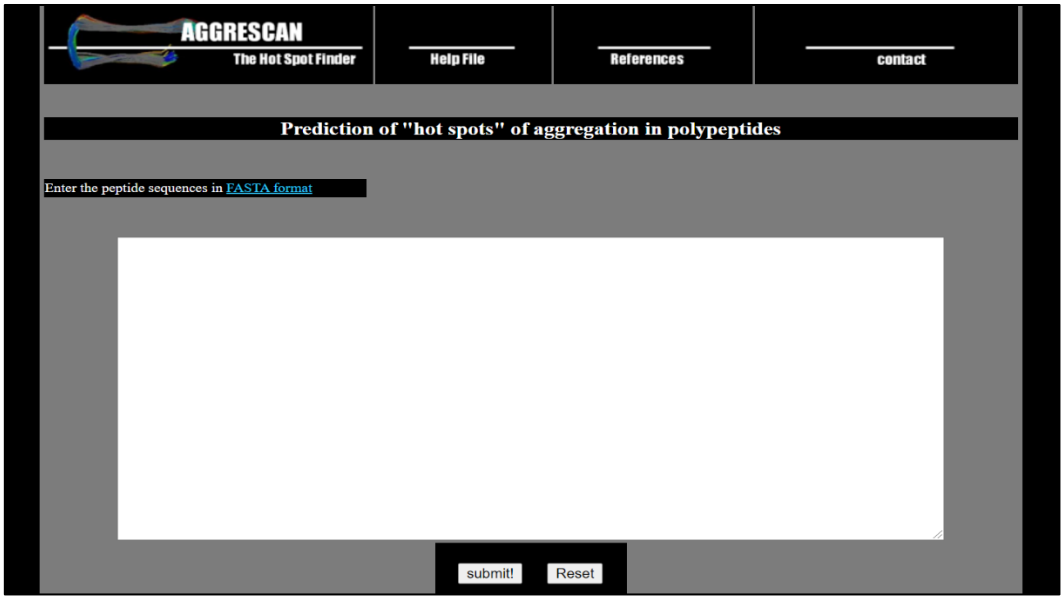

Figure 28: AGGRESCAN protein sequence input window.

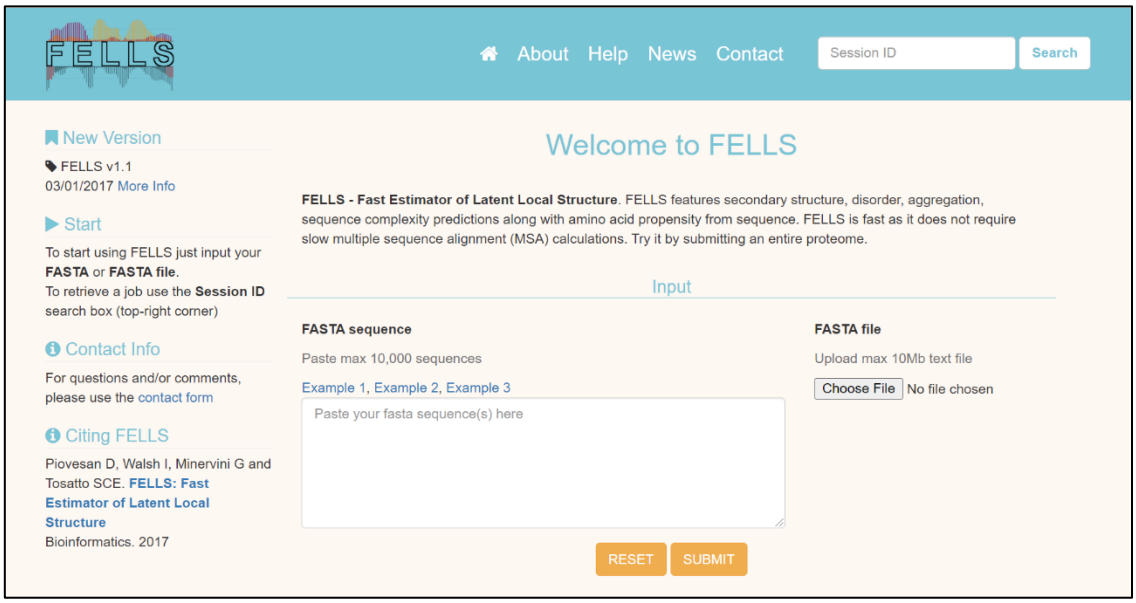

Figure 29: The FELLS protein sequence input window.

4. Results

We used the PASTA 2.0, AGGRESCAN, and FELLS web servers to extract different data which helped characterize the aggregation propensities, the presence of beta-sheets, and the possible location of aggregation prone areas (APRs) also

known as hot spots. AGGRESCAN showed that nearly all of the DBD domains of all 9 main p53 isoforms contained aggregation hot spots as shown in ***Figure* (30 to 38).** Surprisingly, none of the most occurring mutations such as **R175H**, **R248Q**, and **R273H** which occur in the p53 DBD do not fall within these aggregation prone regions. Furthermore, AGGRSCAN shows that many of these aggregation hot spots are clustered next to each other in the DBD of p53. The presence of Proline residues causes a break in the sequence of aggregation prone regions.

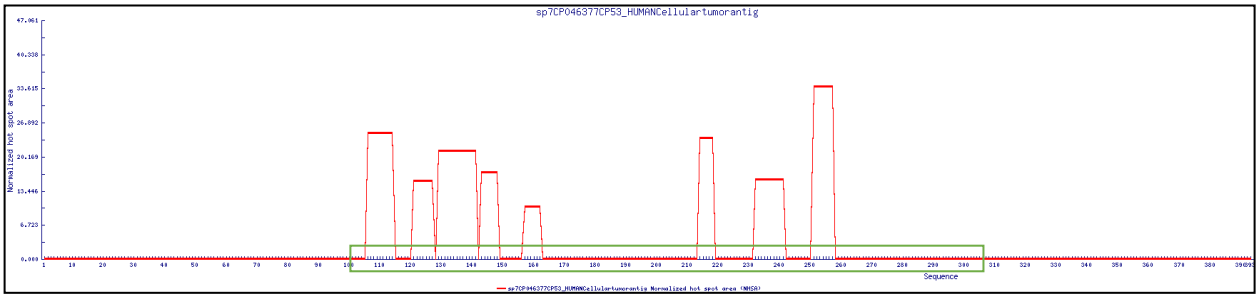

Figure 30: p53 isoform #1 normalized hot spot areas (red squared peaks) and DNA binding domain region (green square).

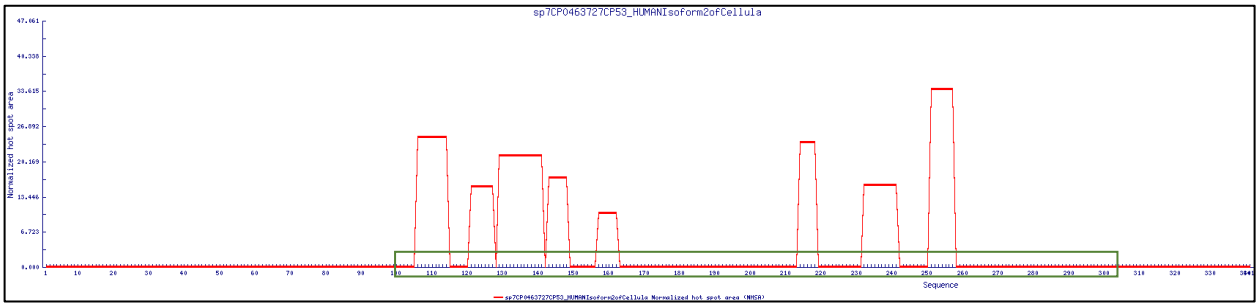

Figure 31: p53 isoform #2 normalized hot spot areas (red squared peaks) and DBD region (green box).

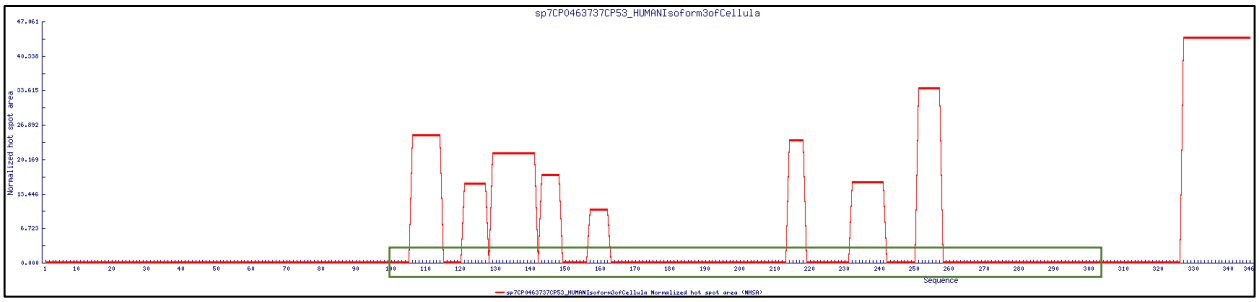

Figure 32: p53 isoform #3 normalized hot spot areas (red squared peaks) and DBD region (green box).

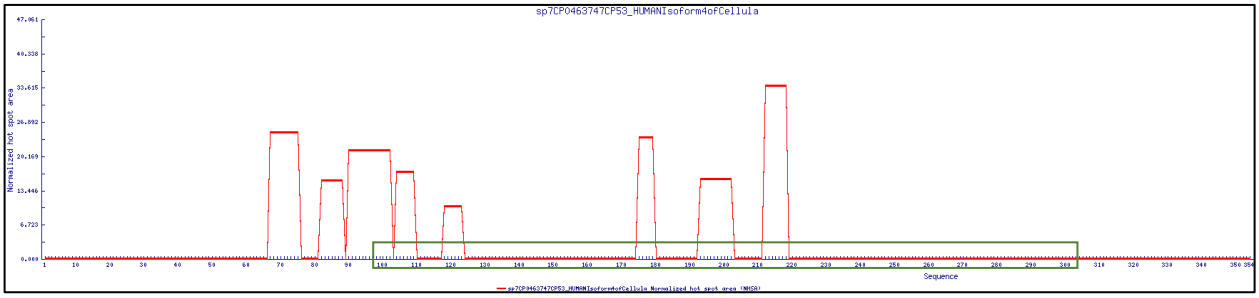

Figure 33: p53 isoform #4 normalized hot spot areas (red squared peaks) and DBD region (green box).

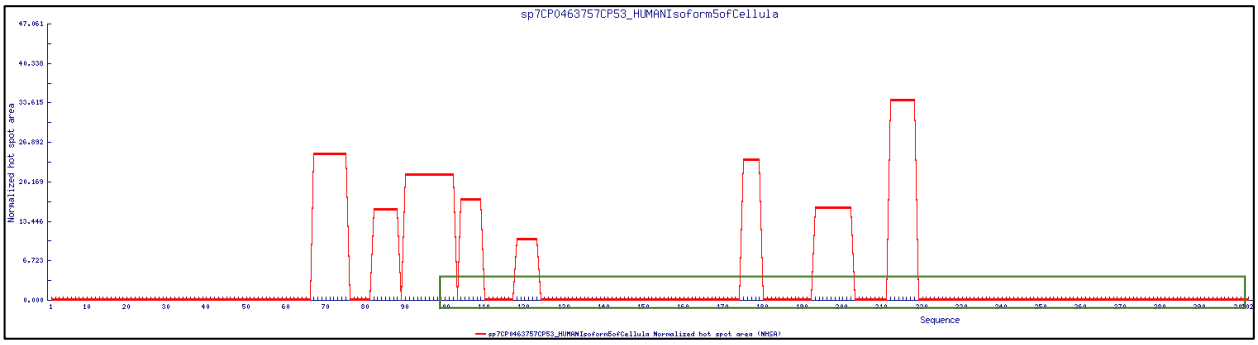

Figure 34: p53 isoform #5 normalized hot spot areas (red squared peaks) and DBD region (green box).

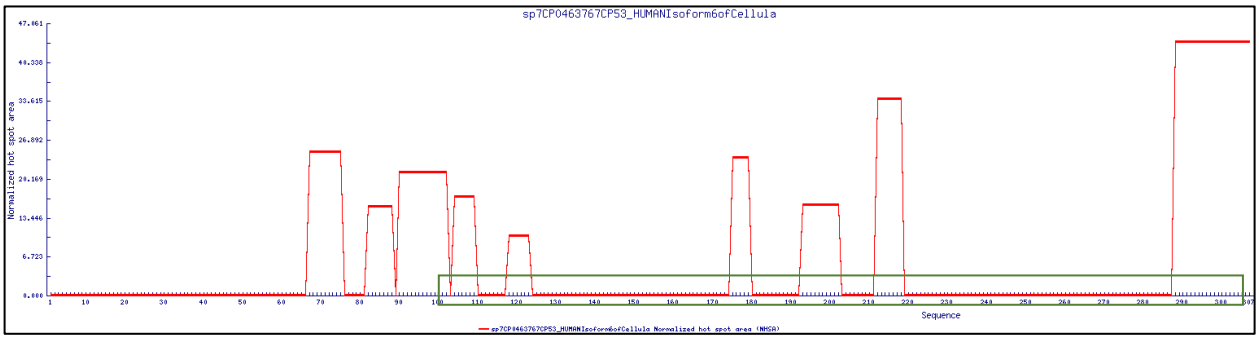

Figure 35: p53 isoform #6 normalized hot spot areas (red squared peaks) and DBD region (green box).

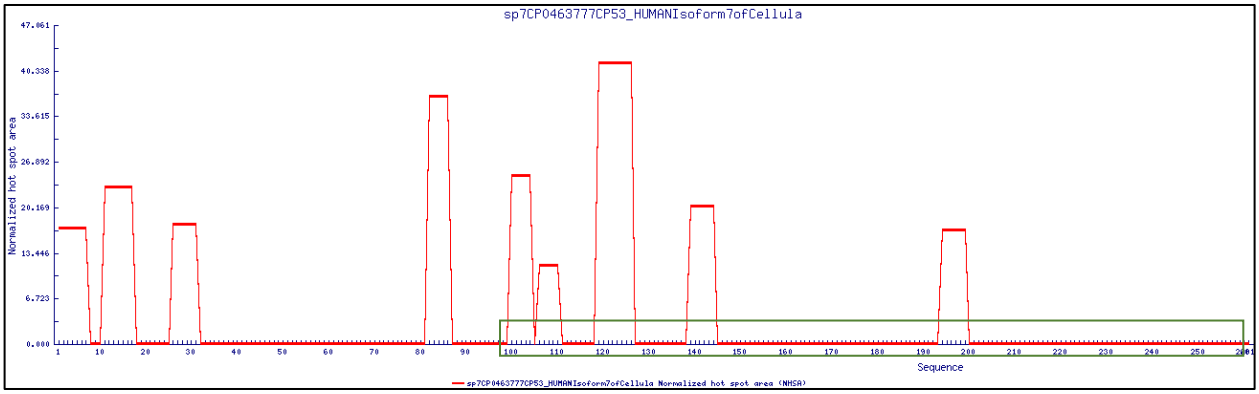

Figure 36: P53 isoform #7 normalized hot pot areas (red squared peaks) and DBD regions (green box).

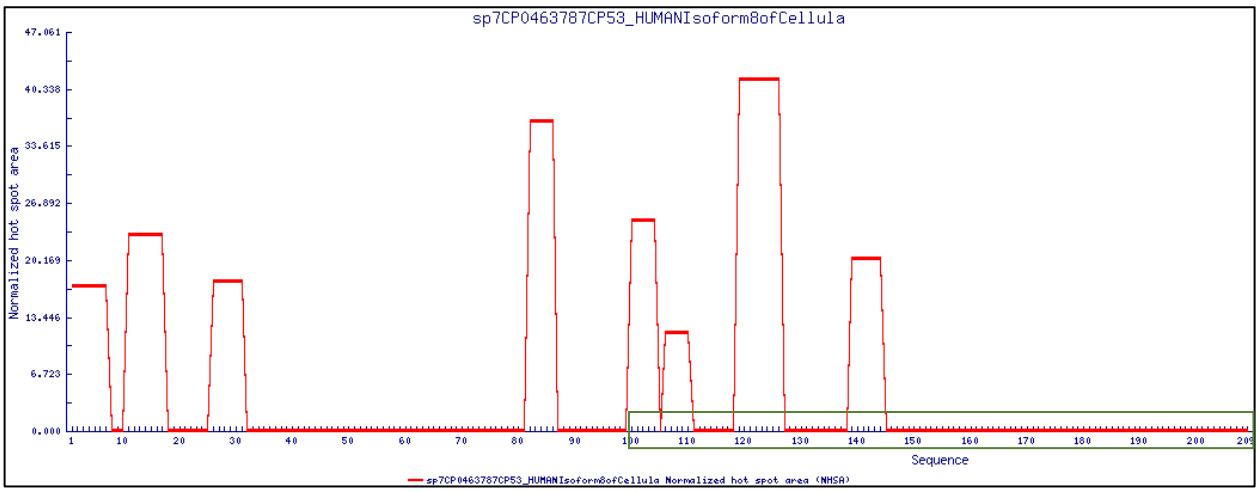

Figure 37: P53 isoform #8 normalized hot spot area (red squared peaks) and DBD region (green box)

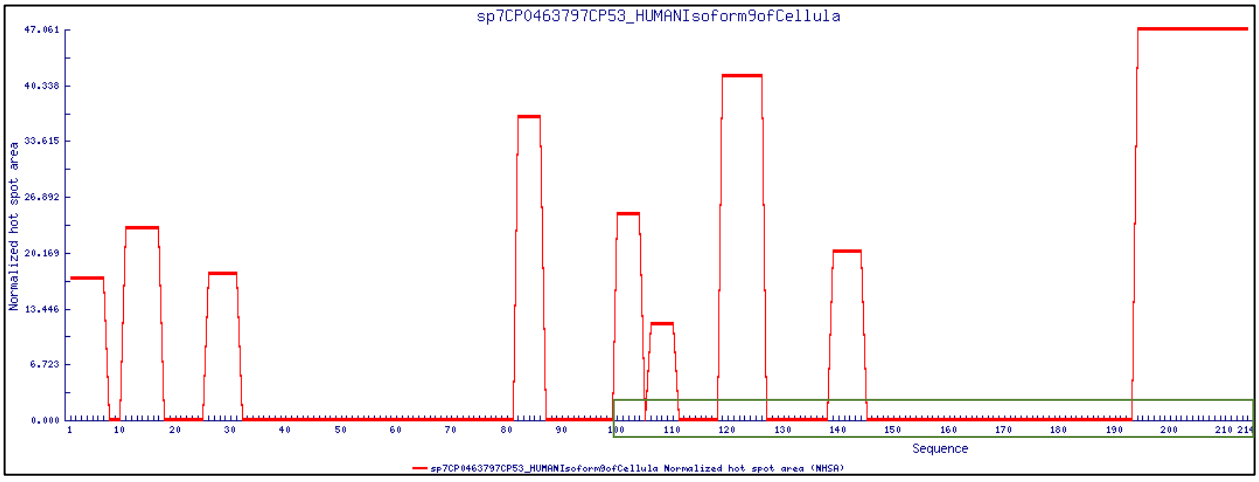

Figure 38: p53 isoform #9 normalized hot spot area (red squared peaks) and DBD region (green box).

Figures (39) to (50) show the AGGRESCAN aggregation prone regions of p63. The p63 protein also a significant number of aggregation hot spots in the DBD regions but unlike p53 the hot stops appear less clustered. For both p53 and p63, the isoforms do not have the same sequence length which is due to the alternative splicing of the p53 and p63 genes. The presence of hot spots in shorter isoform makes the protein less stable as the probability of the APRs of being exposed increases. When the protein conforms to its quaternary structure some of the hot spots end up hidden within the protein and thus have less chance of interacting with DNA or other protein regions.

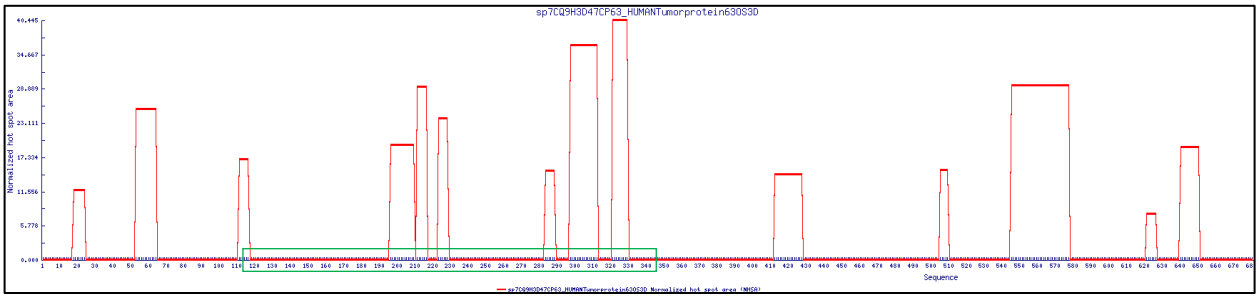

Figure 39: p63 isoform #1 normalized hot spot areas (red squared peaks) DBD (green box).

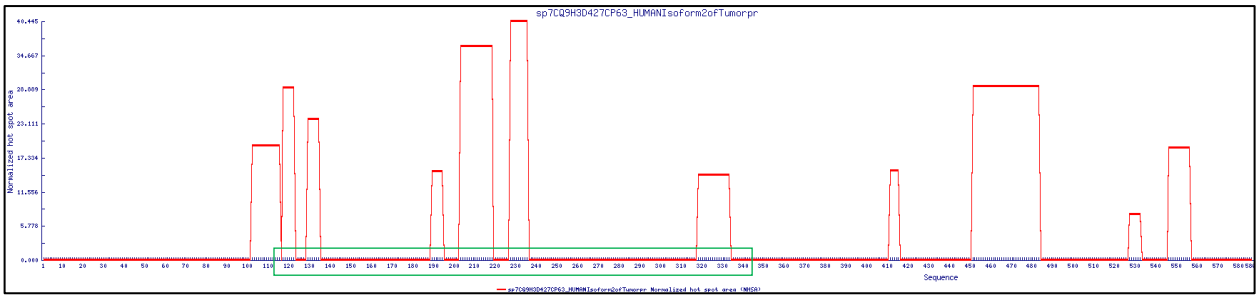

Figure 40: p63 isoform #2 normalized hot spot areas (red squared peaks), DBD (green box).

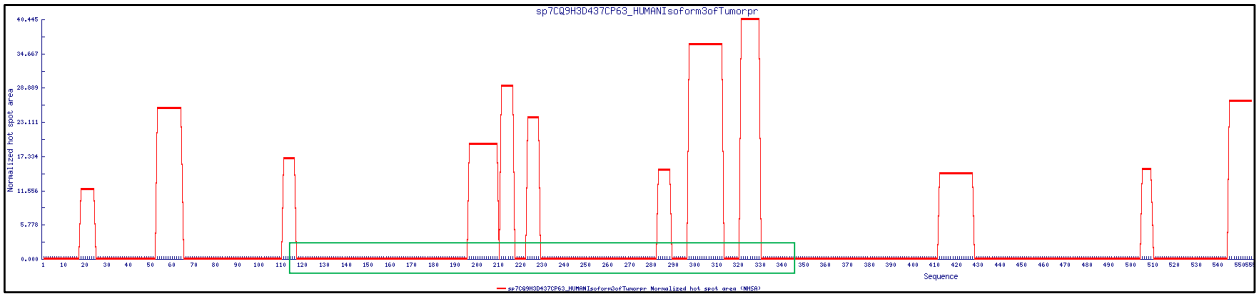

Figure 41: p63 isoform #3 normalized hot spot areas (red squared peaks), DBD (green box).

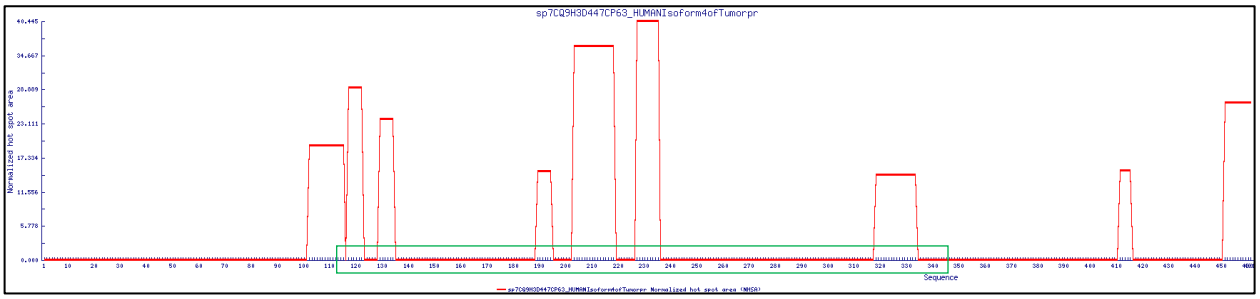

Figure 42: p63 isoform #4 normalized hot spot areas (red squared peaks), DBD (green box).

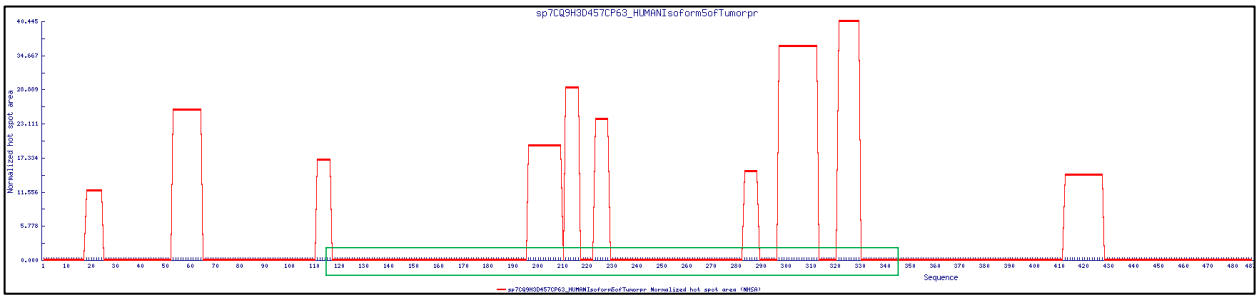

Figure 43: p63 isoform #5 normalized hot spot areas (red squared peaks), DBD (green box).

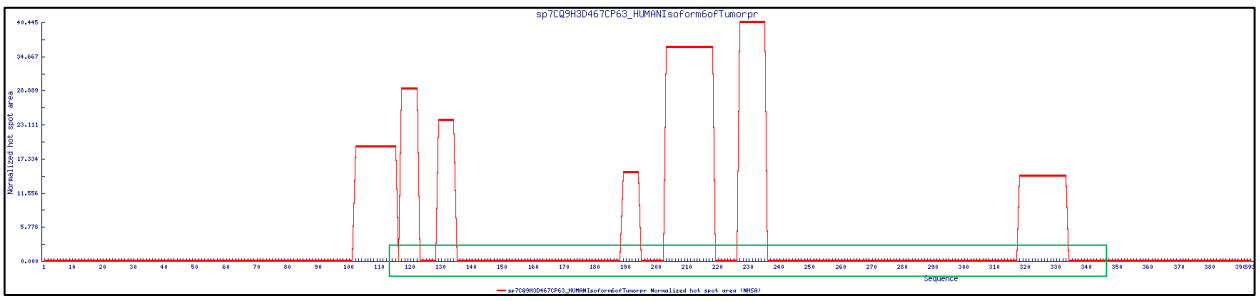

Figure 44: p63 isoform #6 normalized hot spot areas (red squared peaks), DBD (green box).

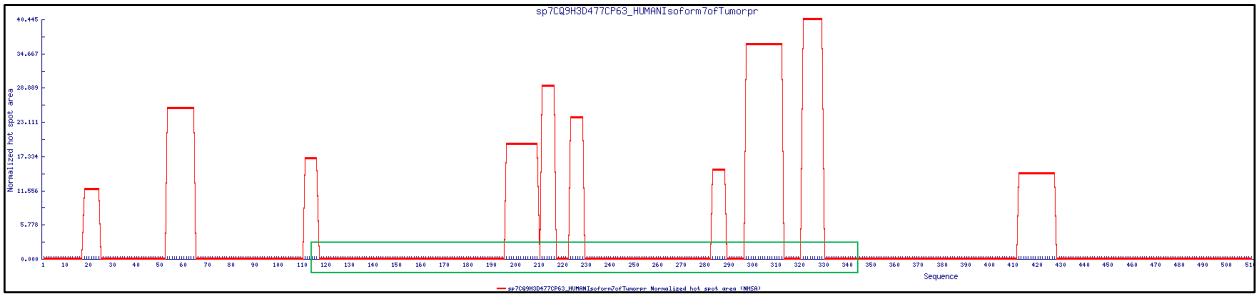

Figure 45: p63 isoform #7 normalized hot spot areas (red squared peaks), DBD (green box).

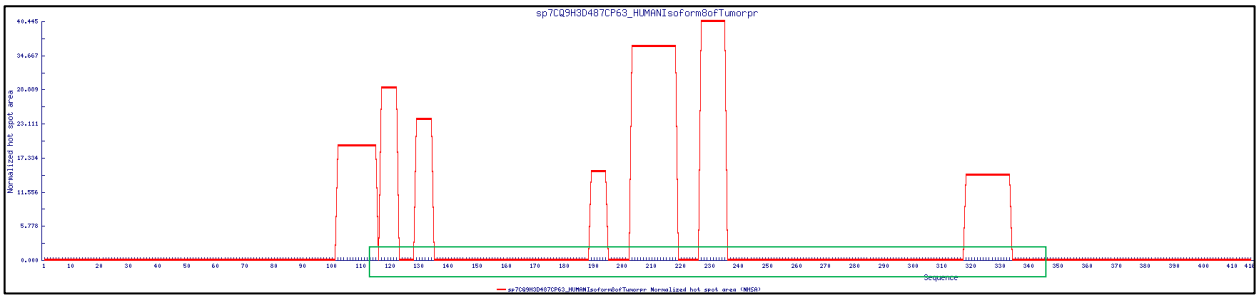

Figure 46: p63 isoform #8 normalized hot spot areas (red squared peaks), DBD (green box).

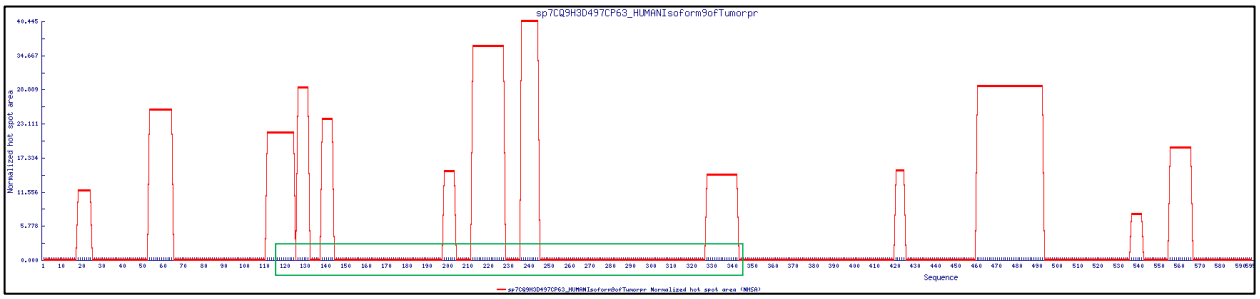

Figure 47: p63 isoform #9 normalized hot spot areas (red squared peaks), DBD (green box).

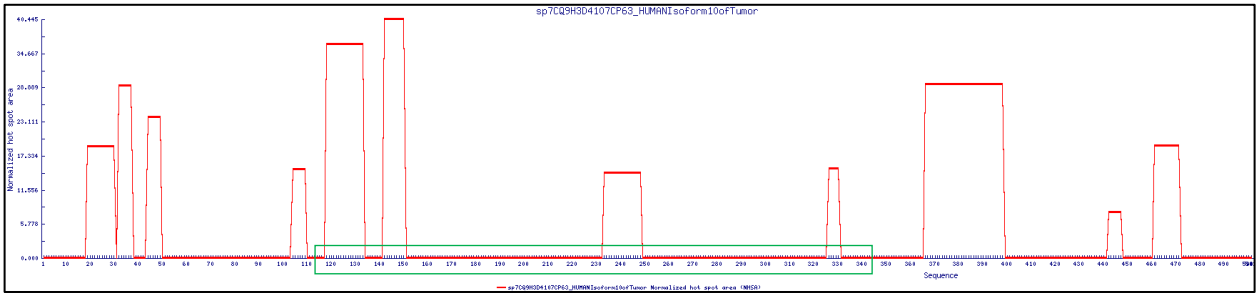

Figure 48: p63 isoform #10 normalized hot spot areas (red squared peaks), DBD (green box).

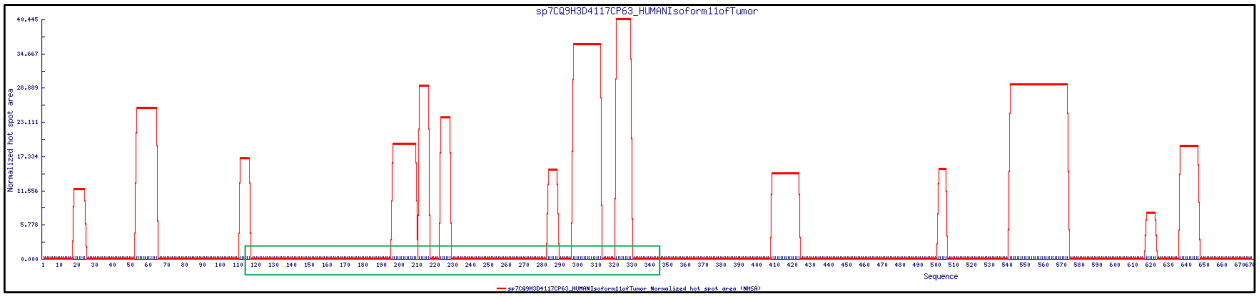

Figure 49: p63 isoform #11 normalized hot spot areas (red squared peaks), DBD (green box).

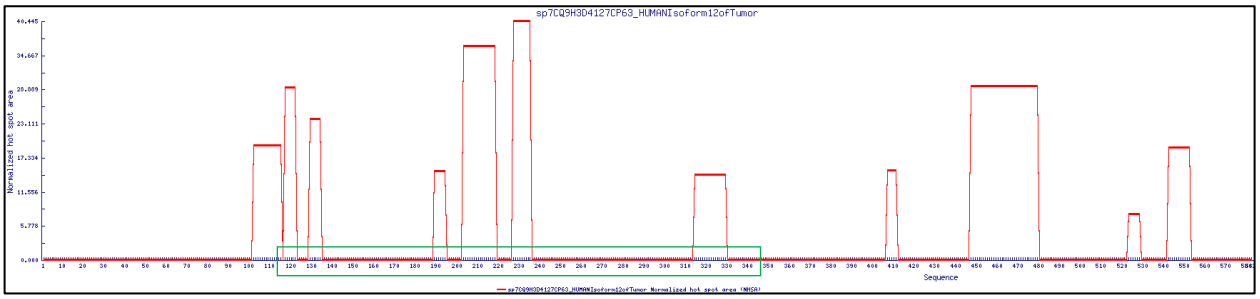

Figure 50: p63 isoform #12 normalized hot spot areas (red squared peaks), DBD (green box).

Results from the FELLS software show that p53 had the highest aggregation percentage of 27.5% covering a total of 108 residues, p63 had the second highest aggregation percentage of 7.9% covering a total of 54 residues, ad third is MDM2 with the least amount of aggregation with 3.7% covering only 18 residues ***Figures (51, 52, 53)***. FELLS also showed less aggregation percentages for shorter isoforms for both p53 and p63 which is expected with shorter sequences. Relative to their protein sequences, p53 has a higher ratio of beta-sheets to residue of 21.6% while p63 has only 12.2%. The increased presence of beta-sheets correlates with the increase in aggregation propensity of p53 as beta-sheets play a major role in inducing protein self and co-aggregation. This correlation does not hold true to for MDM2 as it has 14% of beta-sheets, more than p63, but a lesser aggregation propensity ***Figure (53).***

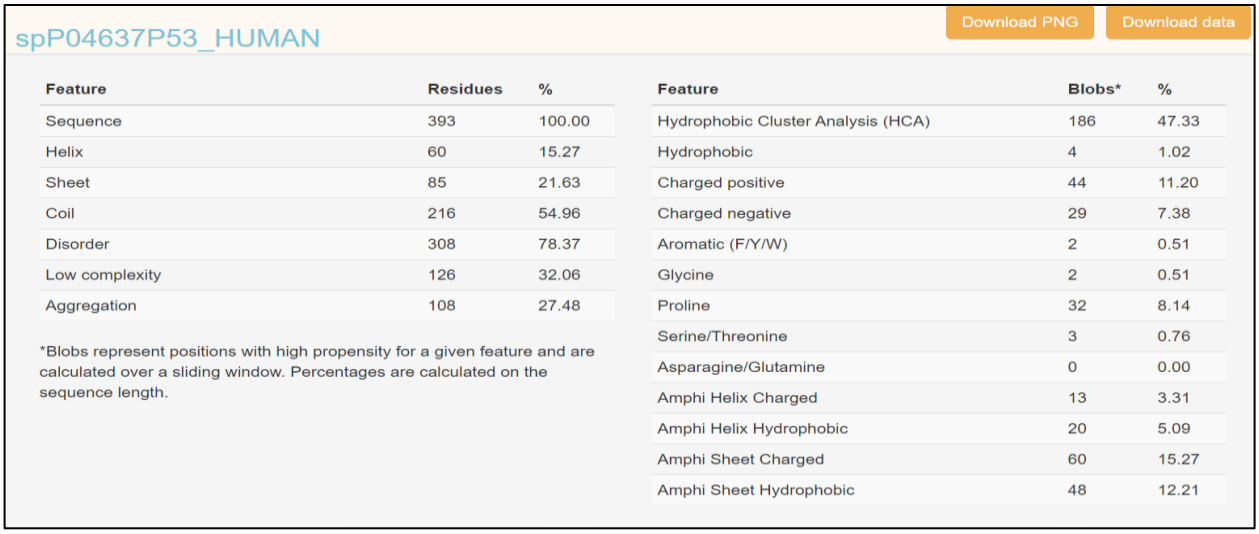

spP04637P53_HUMAN

Download PNG | Download data

Feature	Residues	%
Sequence	393	100.00
Helix	60	15.27
Sheet	85	21.63
Coil	216	54.96
Disorder	308	78.37
Low complexity	126	32.06
Aggregation	108	27.48

*Blobs represent positions with high propensity for a given feature and are calculated over a sliding window. Percentages are calculated on the sequence length.

Feature	Blobs*	%
Hydrophobic Cluster Analysis (HCA)	186	47.33
Hydrophobic	4	1.02
Charged positive	44	11.20
Charged negative	29	7.38
Aromatic (F/Y/W)	2	0.51
Glycine	2	0.51
Proline	32	8.14
Serine/Threonine	3	0.76
Asparagine/Glutamine	0	0.00
Amphi Helix Charged	13	3.31
Amphi Helix Hydrophobic	20	5.09
Amphi Sheet Charged	60	15.27
Amphi Sheet Hydrophobic	48	12.21

Figure 51: Total FELLS structural and aggregation analysis of p53 isoform #1.

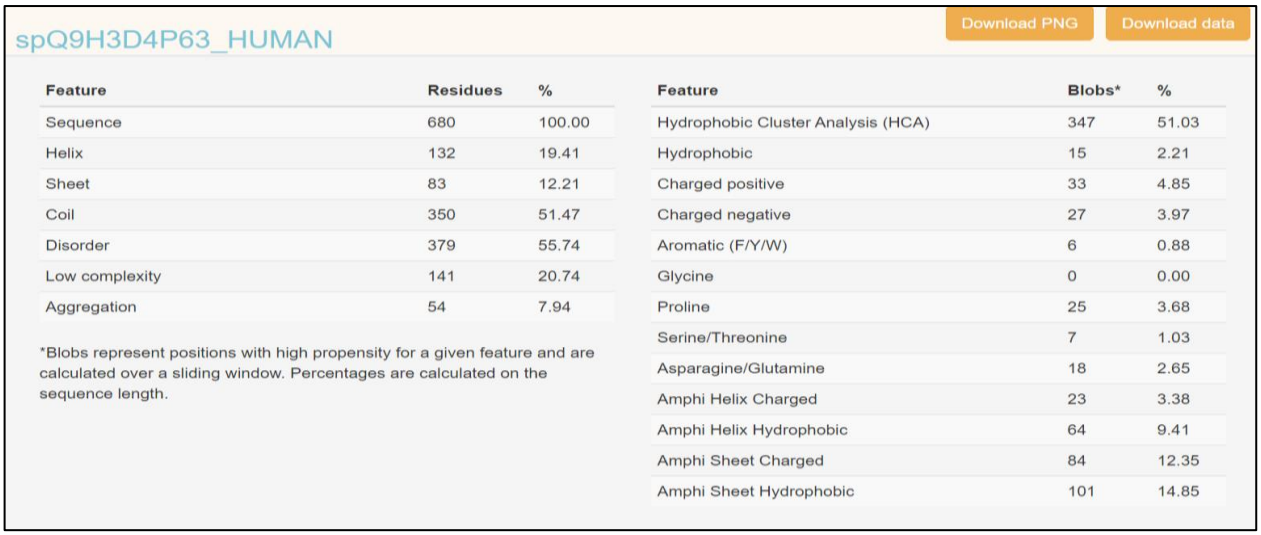

spQ9H3D4P63_HUMAN

Download PNG | Download data

Feature	Residues	%
Sequence	680	100.00
Helix	132	19.41
Sheet	83	12.21
Coil	350	51.47
Disorder	379	55.74
Low complexity	141	20.74
Aggregation	54	7.94

*Blobs represent positions with high propensity for a given feature and are calculated over a sliding window. Percentages are calculated on the sequence length.

Feature	Blobs*	%
Hydrophobic Cluster Analysis (HCA)	347	51.03
Hydrophobic	15	2.21
Charged positive	33	4.85
Charged negative	27	3.97
Aromatic (F/Y/W)	6	0.88
Glycine	0	0.00
Proline	25	3.68
Serine/Threonine	7	1.03
Asparagine/Glutamine	18	2.65
Amphi Helix Charged	23	3.38
Amphi Helix Hydrophobic	64	9.41
Amphi Sheet Charged	84	12.35
Amphi Sheet Hydrophobic	101	14.85

Figure 52: Total FEELs structural and aggregation analysis if p63 isoform #1.

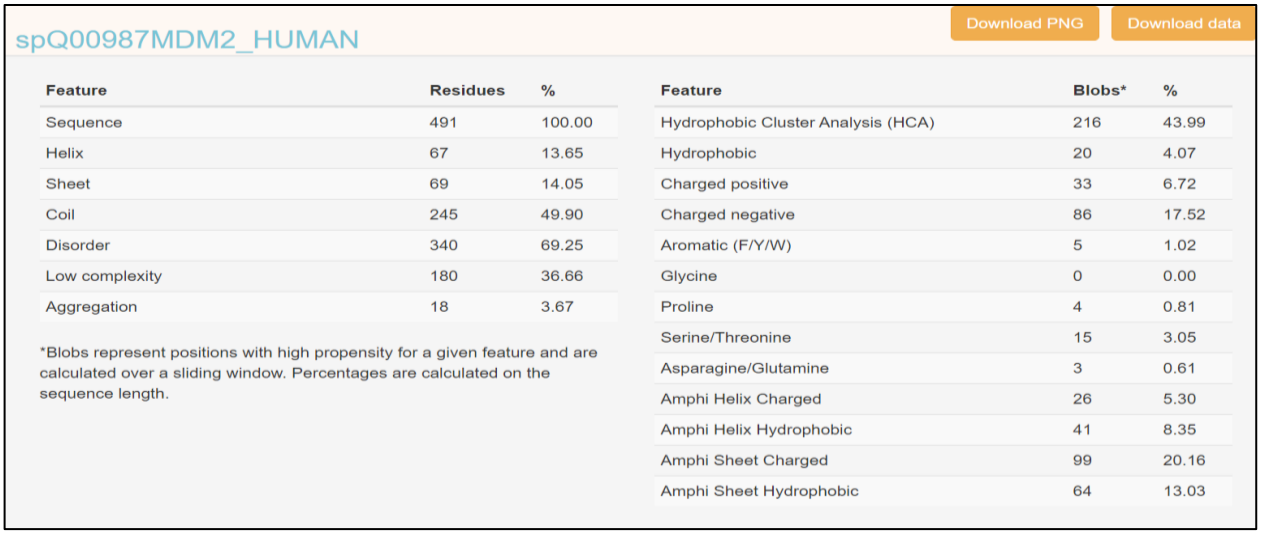

spQ00987MDM2_HUMAN

Download PNG | Download data

Feature	Residues	%
Sequence	491	100.00
Helix	67	13.65
Sheet	69	14.05
Coil	245	49.90
Disorder	340	69.25
Low complexity	180	36.66
Aggregation	18	3.67

*Blobs represent positions with high propensity for a given feature and are calculated over a sliding window. Percentages are calculated on the sequence length.

Feature	Blobs*	%
Hydrophobic Cluster Analysis (HCA)	216	43.99
Hydrophobic	20	4.07
Charged positive	33	6.72
Charged negative	86	17.52
Aromatic (F/Y/W)	5	1.02
Glycine	0	0.00
Proline	4	0.81
Serine/Threonine	15	3.05
Asparagine/Glutamine	3	0.61
Amphi Helix Charged	26	5.30
Amphi Helix Hydrophobic	41	8.35
Amphi Sheet Charged	99	20.16
Amphi Sheet Hydrophobic	64	13.03

Figure 53: Total FELLS structural and aggregation analysis of MDM2 isoform #1.

The hydrophobic cluster analysis (HCA) shown in **Figure (54)** and **(55)** allow the user to delineate the protein amino acid sequence and gain insights about regions of interest which are likely to be ordered under specific conditions as well as disordered regions solely from the amnio acid sequence of the protein. In other words, HCA gives a total picture of the protein's texture with regard to the foldable sequence regions.

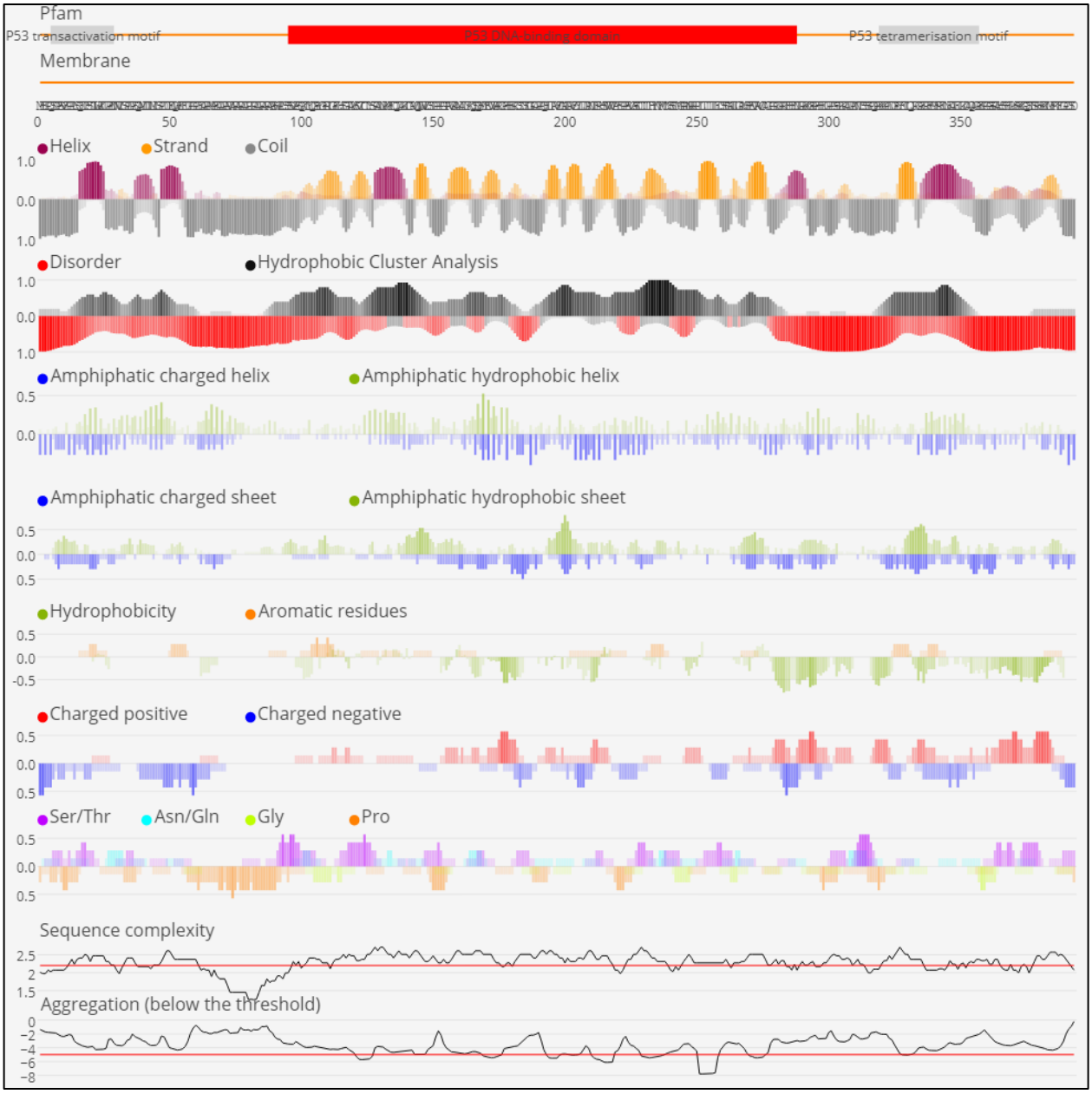

Figure 54: FELLS output for the secondary structure and disorder for p53. p53 DBD has prominent hydrophobic clusters and high number of beta strands.

Figure 55: FELLS output for p63 also showing prominent hydrophobic clusters in the p63 DBD (labeled as p53 DBD due to high homology), the tetramerization motif, and the Sterile Alpha Motif (SAM) domain.

Self-aggregation results showed MDM2 and p63 have the best energies for self-aggregation and this is due partly due to the higher number of possible

amyloids(20 amyloids) than that of p53 (six amyloids). Nonetheless, p53 has the highest percentage of beta-strands ***Figure (56)***.

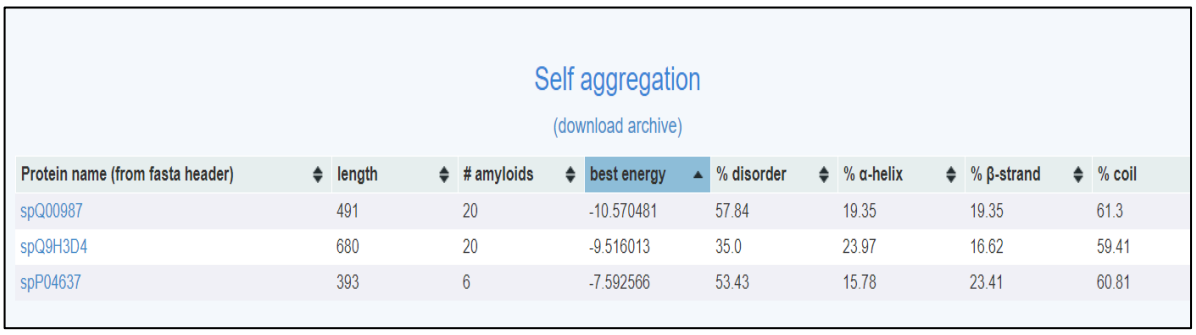

Self aggregation

(download archive)

Protein name (from fasta header)	length	# amyloids	best energy	% disorder	% α-helix	% β-strand	% coil
spQ00987	491	20	-10.570481	57.84	19.35	19.35	61.3
spQ9H3D4	680	20	-9.516013	35.0	23.97	16.62	59.41
spP04637	393	6	-7.592566	53.43	15.78	23.41	60.81

Figure 56: The PASTA 2.0 web server showed that individually, MDM2 (FASTA ID spQ00987) and p63 (FASTA ID spQH3D4) have 20 amyloids each whereas p53 (FASTA ID spP04637) have only six amyloids but a higher percentage (23.41%) of beta-strands.

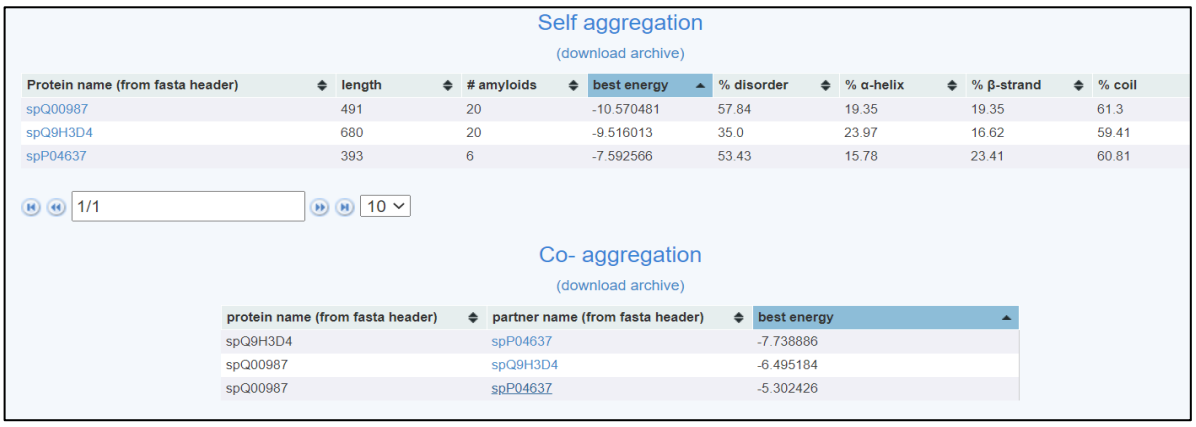

Self aggregation

(download archive)

Protein name (from fasta header)	length	# amyloids	best energy	% disorder	% α-helix	% β-strand	% coil
spQ00987	491	20	-10.570481	57.84	19.35	19.35	61.3
spQ9H3D4	680	20	-9.516013	35.0	23.97	16.62	59.41
spP04637	393	6	-7.592566	53.43	15.78	23.41	60.81

1/1 10

Co- aggregation

(download archive)

protein name (from fasta header)	partner name (from fasta header)	best energy
spQ9H3D4	spP04637	-7.738886
spQ00987	spQ9H3D4	-6.495184
spQ00987	spP04637	-5.302426

Figure 57: The PASTA 2.0 co-aggregation predictions compared with the self-aggregation propensities of p53, p63, and MDM2.

PASTA 2.0 predicted that p53 (FASTA ID spP0437) and MDM2 (FASTA ID spQ00987) have the least energy required (-5.3024626 PASTA units) for co-aggregation whereas p53 and p63 require more energy below aggregation threshold to co-aggregate. ***Figure (58)*** shows that even when mutations happen the

aggregation free energy of p53 remains the same indicating that other factors along mutations induce changes in the aggregation energy of p53.

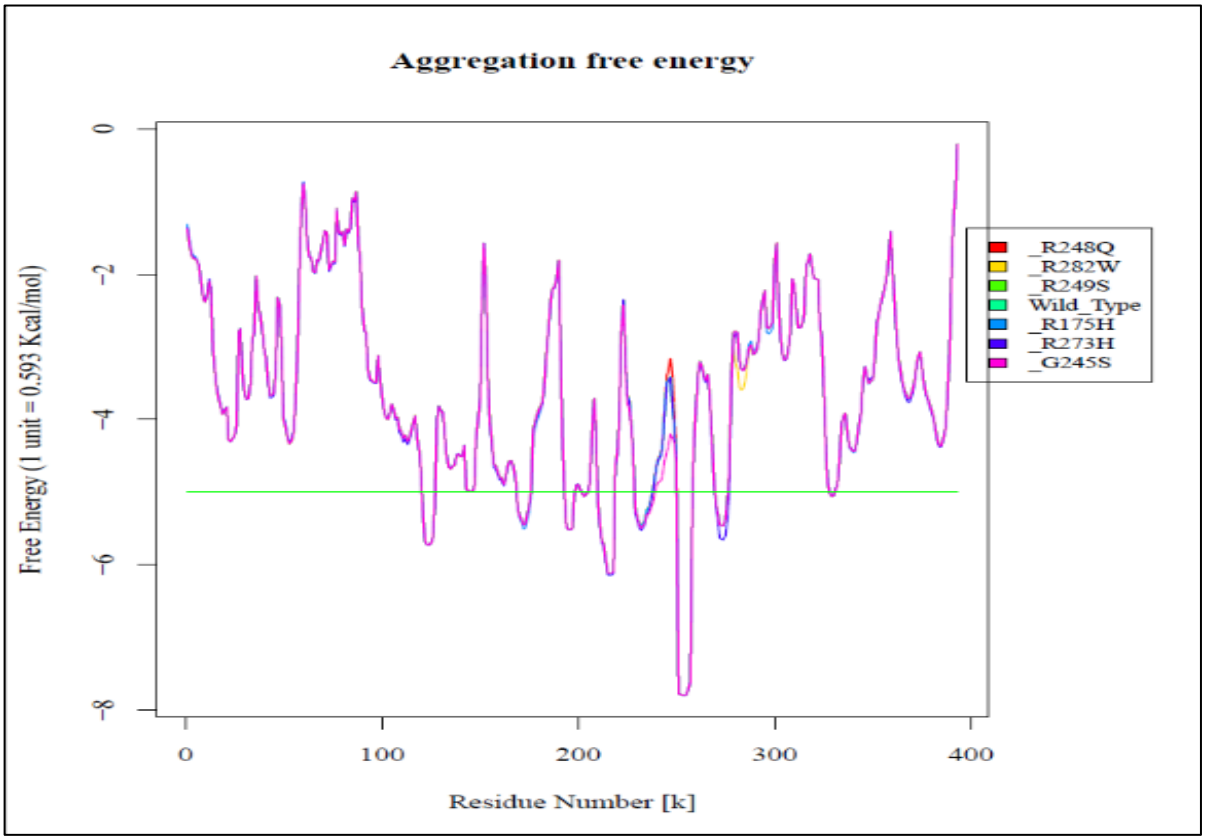

Figure 58: Free Energy graph of six of the some of the most occurring p53 mutations generated via PASA 2.0 (green horizontal line represent the default energy threshold of -5 PASTA where 1 PASTA unit = 0.593 Kcal/mol).

5. Discussion

The tumor suppressing role of p53 is dependent on the p53's structure and its presence in the nucleus. This allows p53 to bind to DNA sequences consequently inducing the activation of other genes sine qua non for DNA stability (Levine, 1997) and (Vousden et al., 2002). In Normal cells, the expression of p53 is strictly regulated leading to a short half-life of 15 to 30 min (Oren et al., 1981).

However, when mutations occur, they prolong the half-life of p53 causing cytoplasmic and nuclear inclusions (Slade and Moll 2003). The p53 DBD contains more that 95% of the cancer-causing missense mutations (Olivier et al., 2002), and this causes p53 to lose its functions via changing the conformation of the DBD and/or decreasing the molecular thermodynamic stability of protein regions. Results from the PASTA 2.0 and the AGGRESCAN web servers yielded different results when predicting the aggregation prone regions. For p53, PASTA 2.0 predicted only one parallel aggregation hot spot from residue 251 to residue 257 (**ILTIITL**). This region is highly conserved in p53 (Ghosh et al., 2014). This However, AGGRESCAN predicted multiple hot spots for p53, which included the conserved region from 251 to 257 (**ILTIITL**), and most of which were clustered in the DBD. It is important to note that mutations rarely occur in the conserved region. One can infer that this conserved region serves as hot spot for the aggregation of wild-type p53 to gain function. Furthermore, Ghosh et al., (2014) state that 327-332 (**YFTLQI**) residue region, another highly conserved region in p53's tetramerization domain, does not aggregate into an amyloid. Our AGGRESCAN results were consist with those of Ghosh et al. (2014) except in the p53 isoform 3 where this region was predicted as a hot spot. Both PASTA 2.0 and FELLS showed a more stable p63 and MDM2 due to their protein length, presence of multiple interactive domains, and highly textured protein region both through the hydrophobic cluster analysis (HCA) and the disordered sequence regions which help with stable protein folding. p53 was shown to be the least stable protein due to its shorter protein length of 393

amino acids, the occurrence of most mutations in its DBD, and also the presence of beta-strands in areas that induce aggregation and protein instability.

Currently, cancer is being considered as an aggregation disease (Bom et al., 2012). During malignancy proteins are uncontrollably expressed with conformational changes. It has been demonstrated that the conformation of the p53 DNA-binding domain (DBD) is unstable (Stindt et al., 2014). Mutations such as R175H, R249S, and R273H additionally destabilize the DBD in p53. Thus, high percentages of these mutant proteins are unfolded and thus inactive. These mutants are found in about 30% of the documented clinical cases and are named “structural” mutants. Furthermore, the gain-of-function (GoF) and the dominant-negative (DN) activity of these structural mutants increase their aggregation tendency (Stindt et al., 2014). Mutations and aggregation alike cause the structural changes that lead to protein instability, the inability to bind DNA and induce gene transactivation, and the loss of function such as the suppression of tumors (Ghosh et al., 2014). Our web-server based analyses, although not confirmatory, showed different aspects of aggregation in p53, p63, and MDM2. Our results showed that there are multiple factors that dictate potential aggregation such as mutations, conserved protein sequences, length of the protein sequence, and the presence of beta-strands and hydrophobic clusters. Our stimulations also show the presence of intrinsic aggregation and amyloidogenic sequences in p53. When wild-type p53, some of these aggregation prone regions are hindered within the folded proteins. Nonetheless, factors such as mutations, stress, and solubility can cause a full-length aggregation of proteins such

as p53 leading to the formation of amyloids and amyloid fibrils. This causes the loss of function and the accumulation of aggregates in cells.

6. References

Aguzzi, A., & O'connor, T. (2010). Protein aggregation diseases: pathogenicity and therapeutic perspectives. *Nature Reviews. Drug Discovery, 9*(3), 237-48. http://dx.doi.org.vortex3.uco.edu/10.1038/nrd3050

Bom APDA, Rangel LP, Costa DCF, et al. Mutant p53 aggregates into prion-like amyloid oligomers and fibrils implications for cancer. J Biol Chem 2012;287:28152–62.

Belyi, V. A, Ak, P, Markert, E, Wang, H, Hu, W, Puzio-Kuter, A, & Levine, A. J. (2009). The Origins and Evolution of the p53 Family of Genes. *Cold Spring Harbor Perspectives in Biology*, *2*(6), a001198–a001198. https://doi.org/10.1101/cshperspect.a001198

Chiti F, Dobson CM. Protein misfolding, functional amyloid, and human disease. Annu Rev Biochem. 2006;75:333-366.doi:10.1146/annurev.biochem.75.101304.123901. PMID: 16756495

Cino, Elio A, Soares, Iaci N, Pedrote, Murilo M, de Oliveira, Guilherme A P, & Silva, Jerson L. (2016). Aggregation tendencies in the p53 family are modulated by backbone hydrogen bonds. *Scientific Reports*, *6*(1), 32535–32535. https://doi.org/10.1038/srep32535

Conchillo-Solé, Oscar, de Groot, Natalia S, Avilés, Francesc X, Vendrell, Josep, Daura, Xavier, & Ventura, Salvador. (2007). AGGRESCAN: a server for the prediction and evaluation of "hot spots" of aggregation in polypeptides. *BMC Bioinformatics*, *8*(1), 65–65. https://doi.org/10.1186/1471-2105-8-65

Dill, K. A, & MacCallum, J. L. (2012). The Protein-Folding Problem, 50 Years On. *Science (American Association for the Advancement of Science)*, *338*(6110), 1042–1046. https://doi.org/10.1126/science.1219021

Freed-Pastor, W. A., & Prives, C. (2012). Mutant p53: one name, many proteins. *Genes & development*, *26*(12), 1268–1286. https://doi.org/10.1101/gad.190678.112

Ghosh, Saikat, Ghosh, Dhiman, Ranganathan, Srivastav, Anoop, A, P, Santosh Kumar, Jha, Narendra Nath, Padinhateeri, Ranjith, & Maji, Samir K. (2014). Investigating the Intrinsic Aggregation Potential of Evolutionarily Conserved Segments in p53. *Biochemistry (Easton)*, *53*(38), 5995–6010. https://doi.org/10.1021/bi500825d

Levine, A. J. (1997). p53, the Cellular Gatekeeper for Growth and Division. *Cell (Cambridge)*, *88*(3), 323–331. https://doi.org/10.1016/s0092-8674(00)81871-1

Olivier, Magali, Eeles, Ros, Hollstein, Monica, Khan, Mohammed A, Harris, Curtis C,& Hainaut, Pierre. (2002). The IARC TP53 database: New online mutation analysis and recommendations to users. *Human Mutation*, *19*(6), 607–614. https://doi.org/10.1002/humu.10081

Oren M, Maltzman W, & Levine A J. (1981). Post-translational regulation of the 54K cellular tumor antigen in normal and transformed cells. *Molecular and Cellular Biology*, *1*(2), 101–110. https://doi.org/10.1128/MCB.1.2.101

Piovesan D, Walsh I, Minervini G, Tosatto SCE. FELLS: fast estimator of latent local structure. Bioinformatics. 2017 Jun 15;33(12):1889-1891. doi:

10.1093/bioinformatics/btx085. PMID: 28186245.

Rangel, Luciana P, Costa, Danielly CF, Vieira, Tuane CRG, & Silva, Jerson L. (2014). The aggregation of mutant p53 produces prion-like properties in cancer. *Prion*, *8*(1), 75–84. https://doi.org/10.4161/pri.27776

Stindt M H, Muller P A J, Ludwig R L, Kehrloesser S, Dötsch V, & K H Vousden. (2014). Functional interplay between MDM2, p63/p73 and mutant p53. Oncogene, Oncogene, 2014.

Santos, Jaime, Pujols, Jordi, Pallarès, Irantzu, Iglesias, Valentín, & Ventura, Salvador. (2020). Computational prediction of protein aggregation: Advances in proteomics, conformation-specific algorithms, and biotechnological applications. *Computational and Structural Biotechnology Journal*, *18*, 1403-1413. https://doi.org/10.1016/j.csbj.2020.05.026

Slade N., Moll U.M. (2003) Mutational Analysis of p53 in Human Tumors. In: Deb S., Deb S.P. (eds) p53 Protocols. Methods in Molecular Biology, vol 234. Springer, Totowa, NJ. https://doi.org/10.1385/1-59259-408-5:231

Vousden, Karen H, & Lu, Xin. (2002). Live or let die: the cell's response to p53. *Nature Reviews. Cancer*, *2*(8), 594–604. https://doi.org/10.1038/nrc864

Walsh, Ian, Seno, Flavio, Tosatto, Silvio C.E, & Trovato, Antonio. (2014). PASTA 2.0: an improved server for protein aggregation prediction. *Nucleic Acids Research*, *42*(W1), W301–W307. https://doi.org/10.1093/nar/gku399

CHAPTER 5: THE POTENTIAL USES OF p53 IN THE AGE ESTIMATION OF ANTERMORTEM AND POSTMORTEM WOUNDS FOR FORENSIC PATHOLOGY APPLICTAIONS.

1. Introduction

In forensic pathology, wound examination is an indispensable practice. It is of great importance to determine the age of a wound and its vitality (Toshikazu 2006). This can correctly determine the age of cutaneous trauma such as wounds, bruises, and scratches. Wound age determination is a classic practice in forensic pathology and remains a challenge to interpret in a forensic-judicial setting (Toshikazu 2006). The healing of a skin wound is a well-orchestrated physiological and anatomical process (Azza et al.,2019). Wound healing consists of three main stages. First is inflammation which last about 48 hours, second is proliferation of cells such fibroblast and keratinocytes, and third is maturation of the skin and tissue (Toshikazu 2006). Hundreds of biological molecules and substances are involved in the process of wound healing (Li et al., 2018). In this summary we focus on the potential use of both p53 to estimate the age of skin injuries such as wounds, bruises, and scratches in a forensic setting. Due to the direct involvement of this protein in skin development and skin cell apoptosis. We proposed a rational that is deduced from previous research findings to present p53 as a potential candidate for the estimation of cutaneous injuries. We also propose that future proteomic tests ought to be developed to complement the existing biomarkers for wound age determination. This rational stems from the way the p53 gene is activated due to cellular stress and damage, how pr53 is expressed, and also degraded before and

after death. p53 is a potential candidates when estimating the age of cutaneous injuries.

2. Summary of Research Findings

Recent progress in forensic scientific techniques has opened the door for many molecules as potential biomarkers for wound age estimation and wound vitality (Li et al., 2018). In recent years, methods such as immunohistochemistry and bottom-up proteomics have been used in forensic pathology and have also been validated by multiple scientific groups (Dettmeyer 2011). Most of the immunohistochemistry studies have focused on inflammatory cells and markers associated with the extracellular matrix such as TNF-α, fibronectin, and IL-6 (Dettmeyer 2011). Wound age estimation is a major aspect in forensic science. Forensic pathologists use wound appearance, scab formation, and subdermal hemorrhage discoloration as indices for wound age estimation (Yagi et al., 2016). Conventional staining methodologies such as the Berlin blue stain can only detect hemosiderin in subdermal tissues seven days post-infliction (Yagi et al., 2016). However, it remains difficult to objectively estimate wound age in the first few 5 days post-infliction (Yagi et al., 2016). Nonetheless, many biomarkers exist, and immunohistochemistry remains a valuable tool to visualize the presence of such biomarkers. Expressed proteins such the Tau protein, interleukins (ILs), and clusters of differentiation (CDs) remain some of the most useful biomarkers in forensic pathology.

The early expression of p53 protein in wounds from thermal wounds from 12 hours to 12 days has been shown (Nagata et al., 1999). In this study and the study by (Taran et al., 2004), the authors investigated whether the expression of p53 can indicate if skin burns in human had taken place ante-mortem or post-mortem. They used immunohistochemistry to quantify the level of p53 expression in burned skin which did assist in the estimation of an ante-mortem burn injury. The normal half-life of p53 protein is in the range of five to 40 minutes (Taran et al., 2004). Hence, p53 does not accumulate in cells due to its rapid degradation (Taran et a., 2004). Nonetheless, the level of p53 can increase once a wound takes place and this is due to DNA damage in the affected area. Once p53 is activated, a tetramer of *wild-type* p53 is formed which stabilizes p53, and consequently allow it to accumulate in cell (SeJin and Seong 2016). Studies such as the one by Taran et al., (2004) used burn wound biopsies from antemortem and postmortem victims and showed that results from living victims cannot be generalized on postmortem wounds. In the antemortem samples, the study showed that high levels of p53 expression in examined epithelia suggest an early wound where peak expression occurred on day two. In the postmortem wounds, peak p53 wound expression was observed in day 77 postmortem. We have shown through the functional interplay between p53 and other proteins necessary for programmed cell death, the p53 expression skin cancer pathologies as well as normal epithelia, and the self-aggregation and co-aggregation of p53, that p53 can potentially be an accurate biomarkers for the determination of cutaneous injuries. This particularly possible in antemortem injuries. Few studies demonstrated a considerable increase in the expression of p53

within the first two day while peak positivity was observed during day nine post injury in antemortem rats (**Figure 59**). The decline of p53 positive cells was shown in antemortem skin injuries on day 23. We also suspect a lesser expression of p53 in postmortem as opposed to antemortem skin trauma.

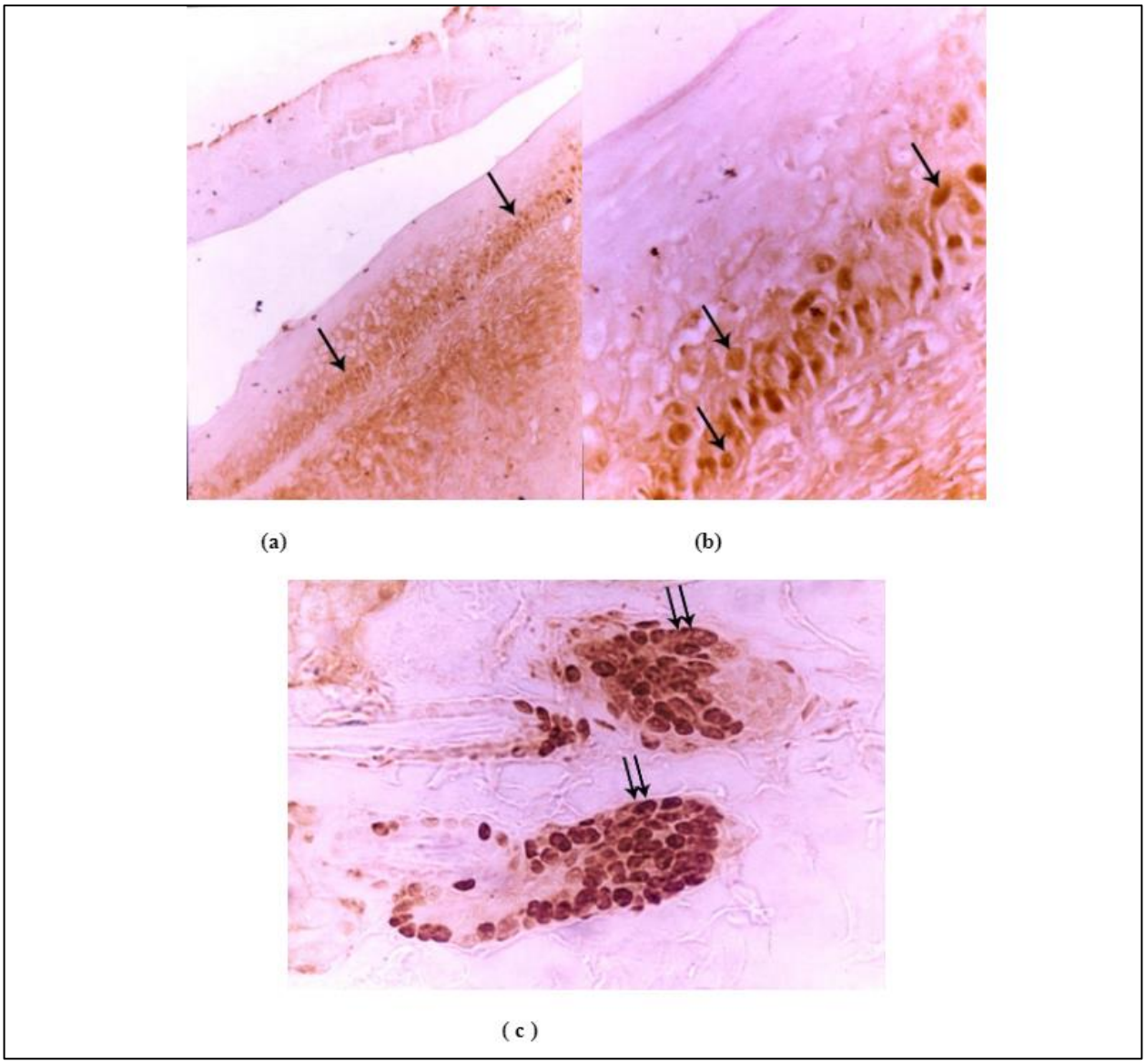

Figure 59: IHC images of skin sections from an adult rat 9 days after a burn injury showing strong p53 nuclear staining in the epithelium basal layer (**a** and **b**), and in the hair follicle (**c**) in the dermis (Taran et al., 2004).

Our literature search did not yield any studies that focus on the application of p63 IHC to determine wound age and wound vitality. This does not rule out p63 as a candidate for future studies. Future research has to focus on the use of the p53 and p63 IHC in the estimation of wound age. This can also be combined with other diagnostic tests such as nucleic acid isolation and amplification (p53 mRNA) from formalin-fixed paraffin-embedded (FFPEs) skin biopsies from both antemortem and postmortem human wounds. Other bottom-up proteomic tests such as protein aggregation assays and staining methodologies such as the Congo Red which is specific for p53 aggregates that are similar in nature to prion amyloid oligomers and fibrils can be complimentary to the p53 IHC of injured skin (Ano et al., 2012). The possibility of multiple methodologies will also provide the investigator the opportunity to validate and reference their findings about timing skin wounds and their vitality both in an antemortem and a postmortem scenario.

3. References

Ano Bom, Ana P D, Rangel, Luciana P, Costa, Danielly C F, de Oliveira, Guilherme A P, Sanches, Daniel, Braga, Carolina A, Gava, Lisandra M, Ramos, Carlos H I, Cepeda, Ana O T, Stumbo, Ana C, De Moura Gallo, Claudia V, Cordeiro, Yraima, & Silva, Jerson L. (2012). Mutant p53 aggregates into prion-like amyloid oligomers and fibrils: implications for cancer. *The Journal of Biological Chemistry*, *287*(33), 28152–28162. https://doi.org/10.1074/jbc.M112.340638

Dettmeyer RB. Vitality, Injury Age, Determination of Skin Wound Age, and Fracture Age. In: Springer, editor. Forensic Histopathology. 1 ed. Berlin: 2011. p. 191-209.

Fouad, Azza, M. M. Badr El Dine, Fatma, M. K. El Dine Menesy, Heba, A. Abdelatif, Amany, & I. Khedr, Rasha. (2019). Detection of the Timing of Human Skin Wounds by Immunohistochemical Analysis of CD14. *Arab Journal of Forensic Sciences & Forensic Medicine*, *1*(10), 1346–1357. https://doi.org/10.26735/16586794.2019.024

Kagawa, Shinichiro, Matsuo, Aya, Yagi, Yoichi, Ikematsu, Kazuya, Tsuda, Ryouichi, & Nakasono, Ichiro. (2009). The time-course analysis of gene expression during wound healing in mouse skin. *Legal Medicine (Tokyo, Japan)*, *11*(2), 70–75. https://doi.org/10.1016/j.legalmed.2008.09.004

Kondo, T. (2006). Timing of skin wounds. *Legal Medicine (Tokyo, Japan)*, *9*(2),

109–114. https://doi.org/10.1016/j.legalmed.2006.11.009

Li, Na, Du, Qiuxiang, Bai, Rufeng, & Sun, Junhong. (2018). Vitality and wound-age estimation in forensic pathology: review and future prospects. *Forensic Sciences Research*, *5*(1), 1–10. https://doi.org/10.1080/20961790.2018.1445441

Nagata M., Takenaka H., Shibagaki R., and Kishimoto S. (1999) Apoptosis and p53 protein expression increases in the process of the burn wound healing in guinea-pig skin. J. Dermatol. 140, 829-38.

SeJin K, Seong S. A. An. Role of p53 Isoforms and Aggregations in Cancer. Medicine, vol. 95, no. 26, 2016, pp. 1

Tarran, Sarah, Dziewulski, Peter, Sztynda, Tamara, & Langlois, Neil E I. (2004). A Study of p53 Expression in Thermal Burns of Human Skin for Determination of Wound Age. *Medicine, Science, and the Law*, *44*(3), 222–226. https://doi.org/10.1258/rsmmsl.44.3.222

Yagi, Yoichi, Murase, Takehiko, Kagawa, Shinichiro, Tsuruya, Shinichiro, Matsuo, Aya, Yamamoto, Takuma, Umehara, Takahiro, & Ikematsu, Kazuya. (2016). Immunohistochemical Detection of CD14 and Combined Assessment with CD32B and CD68 for Wound Age Estimation. *Forensic Science International*, *262*, 113–120. https://doi.org/10.1016/j.forsciint.2016.02.031